

# Electrokinetics over charge-modulated surfaces in the presence of patterned wettability: Role of the anisotropic streaming potential

Uddipta Ghosh and Suman Chakraborty\*

*Department of Mechanical Engineering, Indian Institute of Technology, Kharagpur 721302, India*

(Received 9 April 2013; published 4 September 2013)

In the present study, we focus on evaluating the induced streaming electric field along the orthogonal directions in a narrow fluidic confinement in the presence of patterned surface wettability and modulated surface charges. We attempt to assess the implications of such modulations on the related important quantities and pinpoint the regimes of improved induced streaming potential field and the resulting anisotropy in the induced potential. Our results reveal that for certain combinations of the parameters characterizing the modulated slip, a significant amount of augmentation in the streaming electric field might be obtained, whereas in other cases the effects may lead to adverse consequences. We further demonstrate that the presence of anisotropic modulations on the channel walls give rise to considerable off-diagonal effects, which makes the streaming potential “disoriented” with the applied pressure gradient, when the same is not applied along one of the orthogonal directions. Our analysis also shows that one can remove such “mis-orientations” by finely tuning several relevant flow and geometric parameters, which may bear immense scientific and technological consequences towards an improved design of miniaturized energy conversion devices.

DOI: [10.1103/PhysRevE.88.033001](https://doi.org/10.1103/PhysRevE.88.033001)

PACS number(s): 47.61.–k

## I. INTRODUCTION

Energy harvesting through employing fluid flow in miniaturized devices has been a topic of great interest in the past few years. One possible underlying mechanism governing the same involves the exploitation of streaming potential [1] in a pressure driven flow field having surplus ionic species of either positive or negative charges, which converts the hydrodynamic energy of a pressure driven flow into a net induced electrical potential. This phenomenon exploits the fact that, because of complex electrochemical interactions, a net charge may be induced at the interface (say solid-liquid interface, for example) of two phases. In an effort to maintain overall electroneutrality, a net charge of the opposite sign is induced in the fluid, which is considered to be confined within a charged interfacial fluid layer (consisting of a fixed as well as a mobile layer of charges), also known as the electric double layer [2] (EDL). When a net transport of the fluid is created by an externally applied force (e.g., pressure gradient), the charges are transported along with the fluid, which creates a net current (also called streaming current) in the fluid. This, in turn, leads to a dynamic accumulation of charges in the downstream region, which induces a net potential of its own in order to render the net current zero, which can be used to convert hydrodynamic energy to electrical energy.

A number of theoretical [1,3–18] and experimental [19,20] investigations on the evaluation of streaming potential and energy conversion through streaming potential have previously been executed, and the corresponding energy conversion efficiencies have also been evaluated. Though theoretical estimates show that the conversion efficiency for Newtonian fluids [8] can go as high as 50%, experimental values of the conversion efficiency for the same fluids have been demonstrated to be on the order of [19] 1%–5% in microchannels. Marginally improved values of energy conversion

efficiencies (as high as 12%) have been realized for nanofluidic channels exploiting EDL overlap phenomenon [19]. Recently, Bandyopadhyay and Chakraborty [4–6] demonstrated that by employing viscoelastic fluids, one may dramatically augment the energy conversion efficiency.

Recent studies [8,10] show that, by realizing interfacial slip, one can greatly augment the flow rate and hence the resulting streaming current, which also results in a relative augmentation in the induced streaming potential and hence the energy conversion efficiency. In addition to this, recent advancements in the field of microfabrication have also led to the development of a number of new methods [21–33] of implementing varying surface wettability on microchannel walls, which include various physical [27–29] and chemical techniques [30–33]. Variation in surface properties is also likely to trigger variation in the surface potential, which, in conjunction with the axially varying wettability, might give rise to a plethora of intriguing flow physics. It is interesting to note that such inhomogeneities might also be obtained from topographically varying surfaces [34–37]. Electro-osmotic and pressure driven flows in the presence of topographically and charge-modulated surfaces have previously been investigated by a number of researchers [34–45] and have been shown to have useful applications in mixing [34,41–44]. Pressure driven [46–48] and electrokinetically [34,49–51] driven flows in the presence of modulated surface wettability have also been studied by a number of previous researchers. Brunet and Ajdari [35] have investigated the streaming currents in the presence of topographical and charge modulations on the surfaces and have shown that the resulting net streaming currents are much smaller than the corresponding values generated from an axially homogeneous surface potential.

In recent years, researchers have realized that the implementation of patterned surface conditions (both topographical and chemical) might lead to anisotropy in the nature of the flow, thus making the net throughput strongly dependent on the direction of the applied driving force. A number of recent studies [36,49,52–58] have executed thorough investigations

\*Corresponding author: [suman@mech.iitkgp.ernet.in](mailto:suman@mech.iitkgp.ernet.in)

on this phenomenon over anisotropic surfaces, i.e., for surfaces with variation in wettability (or topography) in a preferred direction. These studies demonstrate that, for flows over such surfaces, i.e., surfaces with predefined orthogonal directions, the flow direction is somewhat shifted from the direction of the driving force [36,49,52–58]. Extrapolating this idea, one can also infer that the induced streaming potential as a result of such physical paradigm might also have off-diagonal components as the streaming current, which is somewhat analogous to the net throughput, is likely to exist in a direction other than that of the driving pressure gradient. In this respect, it should be noted that the direction of the flow will be in the same direction as the driving force when the channel is bounded from the lateral directions. However, in the present study we have considered a channel open in both the lateral and the longitudinal directions (please refer to Fig. 1), which allow the flow to take place in both the directions and thus the possibility of misalignment of flow direction and the direction of the driving force remains. In fact, as depicted in our results, it is this feature of the channel which brings anisotropy into the picture. Considerations of such channels, i.e., channels open in both longitudinal and lateral directions, are nothing new as several previous researchers [36,49,52–58] have investigated the extent of anisotropy in channels with patterned walls (both topographical and chemical patterning). Additionally, a number of studies have also been dedicated to finding out the effective slip for surfaces with a wettability patch of predefined slip length, with given orthogonal directions, for pressure driven [48,53,54,58] as well as electro-osmotically driven flows [49,50,55], albeit mostly for a single surface without the effects of confinements. In a few of the recent studies [50,53,54] it has been demonstrated that such an effective slip can also be defined for a confinement for various kinds of flow actuation mechanisms. Streaming potential calculation, for flows over surfaces with patches of wettability and potential, has previously been executed by Zhao [59], although the effects of confinements were not investigated in that study. Previously, Ajdari [36,37,52] investigated the effects of anisotropic topographical modulations on streaming current and net throughput in the regime of thin double layers with channel walls bearing modulated potential. Nevertheless, a close review of the related literature shows that the effects of anisotropically patterned slip in presence of modulated surface charge on the streaming potential induced in a narrow fluidic confinement is yet to be properly addressed by the research community.

In the present study, we focus on the various aspects of streaming potential generated by virtue of an applied pressure gradient in a narrow fluidic confinement with modulated surface potential and axially varying surface wettability (characterized by an axially modulated Navier slip coefficient). We evaluate the induced streaming potential in both the orthogonal directions and thereafter quantify the extent of anisotropy in the flow through the variation in the angular shift in the streaming potential from the direction of the applied pressure gradient. We also present a general expression for the induced potential for an applied pressure gradient at any arbitrary angle with one of the orthogonal directions of the channel. We further note that in cases of channels consisting of lateral walls, an additional pressure gradient will be induced along the lateral direction, which will render the net flow in that direction to zero. Ajdari

[52] has previously evaluated the induced pressure gradient in the transverse direction, generated from an axially applied pressure gradient, over a topographically undulated surface. It thus follows that, for closed channels, this additionally induced pressure gradient will induce a streaming electric field of its own, which will act in tandem with the induced field of the external gradient. We address the presence of sidewalls in more detail in the mathematical formalism and further show that the possibility of a shift in the direction of the induced field exists in these cases as well. However, while reporting our results, we consider a channel, which is open in both longitudinal and lateral directions (refer to Fig. 1) and hence we do not take into account any such induced pressure gradient. In an effort to adhere to an elegant analytical framework without sacrificing the essential physics, we use the Debye-Hückel linearization for the calculation of the corresponding electrostatic field and the ion distributions. Our analysis reveals that in some cases the employment of the modulated slip and potential result in augmentation in the desired effects, whereas in other cases the imposed perturbations may act unfavorably. We also demonstrate that the extent of anisotropy can be controlled by adjusting various flow parameters to the extent that the induced potential can be aligned exactly with the applied pressure gradient acting in any arbitrary direction.

## II. MATHEMATICAL MODEL

As a physical system appropriate to the present study, we consider a channel of slit-type geometry, with the channel height being  $H$  and width  $w$ , being much larger than the channel height. The origin is placed on the bottom wall, where the  $x$  axis runs along the channel in the axial direction and the  $y$  axis runs vertically so that the plates are positioned at  $y = 0$  and  $H$ . The channel walls bear modulated surface potential, mathematically expressed as  $\psi(y = 0, H) = \zeta_0[1 + m \cos(qx)]$ . This potential is assumed to be low enough so that the Debye-Hückel linearization can be safely applied. The channel walls also bear axially modulated slip, given by (a) on the bottom wall,  $l_s[1 + \delta \cos(qx + \theta)]$ ; (b) on the top wall,  $l_s[1 + n\delta \cos(qx + \theta)]$ , which makes the slip differing in phase with the surface potential. The fluid viscosity, permittivity, and density are taken to be,  $\mu$ ,  $\epsilon$ , and  $\rho$ , respectively. It is clear from the description of the geometry that the modulations run parallel to the  $z$  axis and perpendicular to the  $x$  axis. This indicates that the two orthogonal directions in the channel under consideration are  $x$  and  $z$  axes. We name  $x$  to be the perpendicular and  $z$  to be the parallel orthogonal directions. In the present analysis, we first attempt to determine the induced potential field for applied pressure gradients in these two orthogonal directions. We can combine the induced fields in these two directions to determine the total streaming potential for any applied pressure gradient, which is not oriented along the orthogonal directions.

### A. Applied pressure gradient in the $x$ (perpendicular) direction

#### 1. Pressure driven flow

A pressure gradient of magnitude  $\Omega^\perp$  along the  $x$  direction in the channel is applied in order to actuate the flow. As mentioned earlier, the presence of the charge in the

channel induces a streaming current, which, in turn, induces a streaming potential and is mathematically denoted by  $E_0^\perp$ . Pressure driven flow in microconfinements in the presence of modulated slip as described in the present study, has previously been investigated by Hendy *et al.* [46], from continuum as well as molecular dynamics considerations. However, we rederive the resulting velocity profiles with an assumption of low Reynolds number flow, thus neglecting the inertial terms in the Navier-Stokes equation. The equations, combining the effects of the induced electric field, are given by

$$-\frac{\partial p}{\partial x} + \mu \nabla^2 u^\perp + \rho_e E_0^\perp = 0, \quad (1a)$$

$$-\frac{\partial p}{\partial y} + \mu \nabla^2 v^\perp = 0, \quad (1b)$$

$$\nabla \cdot \mathbf{v}^\perp = 0. \quad (1c)$$

It is important to mention here that despite no application of any external electric field, an electrical body force appears in Eq. (1a), as attributable to the establishment of a streaming electric field,  $E_0$ . Further, it is important to note that in Eqs. (1a)–(1b), the pressure gradient terms are combined consequences of the applied and the induced pressure gradients (as attributed to modulated surface conditions).

Since Eqs. (1a) and (1b) are linear, we can separate out the contributions from the electrokinetic flow and the pressure driven flow in the following way:  $\mathbf{v}^\perp = \mathbf{v}_p^\perp + \mathbf{v}_e^\perp$ , where  $p$  and  $e$  denote contributions from pressure gradient and electric field, respectively. The equation for  $\mathbf{v}_p^\perp$  in a nondimensional form is given by

$$-\frac{\partial p}{\partial x} + \nabla^2 u_p^\perp = 0, \quad (2a)$$

$$-\frac{\partial p}{\partial y} + \nabla^2 v_p^\perp = 0, \quad (2b)$$

$$\nabla \cdot \mathbf{v}_p^\perp = 0. \quad (2c)$$

The variables in Eqs. (2a)–(2c) have been nondimensionalized as follows:  $u_p, v_p \rightarrow \frac{u_p}{u_{p,\text{ref}}}, \frac{v_p}{u_{p,\text{ref}}}$ ;  $x, y \rightarrow \frac{x}{H}, \frac{y}{H}$ ;  $p \rightarrow \frac{p}{(\Omega H)}$ . Here,  $u_{p,\text{ref}} = \frac{H^2 \Omega^\perp}{\mu}$ . We have not used any separate symbol for the nondimensional variables as we use these variables all along in our analysis from now onward. The boundary

conditions for the velocity are specified by

$$u_p^\perp(0) = l_s [1 + \delta \cos(qx + \theta)] \frac{\partial u_p^\perp(y=0)}{\partial y}$$

and

$$u_p^\perp(1) = -l_s [1 + n\delta \cos(qx + \theta)] \frac{\partial u_p^\perp(y=1)}{\partial y}, \quad (3a)$$

$$v_p^\perp(0) = 0, \quad \text{and} \quad v_p^\perp(1) = 0. \quad (3b)$$

Note that here  $l_s \rightarrow l_s/H$ ;  $q \rightarrow qH$ , after normalization. Equations (2a)–(2c) can be analytically solved subjected to the boundary conditions (3a) and (3b) using regular perturbation method, where a variable  $\xi$  can be expressed as

$$\xi = \xi^{(0)} + \delta \xi^{(1)} + \delta^2 \xi^{(2)} + O(\delta^3). \quad (4)$$

Here,  $\xi$  can represent variables like,  $\mathbf{v}_p$ ,  $p$ ,  $\mathbf{v}_e$ , etc. In this respect, it should be noted that the slip modulation amplitude for the upper wall is  $n\delta$  and hence, ideally, we should consider perturbation variable to be  $n\delta$  instead of  $\delta$ , for  $n > 1$ . However, in the present analysis, we consider only three values of  $n = 1, 0$ , and  $-1$ . This makes the amplitude of slip modulation on the top wall either equal to that of the bottom wall or zero. Therefore, we can expand the relevant variables using only  $\delta$  as the perturbation parameter. Using the solution of the form described in Eq. (4), one can solve Eqs. (2a)–(2c) by invoking a stream function, to get a solution of the form

$$u_p^\perp = u_p^{\perp(0)} + \delta u_p^{\perp(1)} + \delta^2 u_p^{\perp(2)} + O(\delta^3), \quad (5a)$$

where

$$u_p^{\perp(0)} = \frac{1}{2} \{y(1-y) + l_s\}, \quad (5b)$$

$$u_p^{\perp(1)} = g_p^{\perp(1)}(y) \cos(qx + \theta), \quad (5c)$$

$$u_p^{\perp(2)} = K_1 y + K_2 + g_p^{\perp(2)}(y) \cos(2qx + 2\theta). \quad (5d)$$

Here,  $g' = \frac{dg}{dy}$ . The functions  $g'$ 's are defined by

$$g_p^i = a_1^i y \cosh(iqy) + (a_2^i + a_3^i y) \sinh(iqy), \quad i = 1, 2, \quad (5e)$$

$$\Gamma(i) \hat{a}^i = \hat{C}_i, \quad \hat{a}_i = [a_1^i a_2^i a_3^i]^T, \quad i = 1, 2, \quad (5f)$$

where, the matrices are defined as

$$\Gamma(i) = \begin{bmatrix} \cosh(iq) & \sinh(iq) & \sinh(iq) \\ 1 & iq & 2iq l_s \\ iq \sinh(iq) + \cosh(iq) & iq \cosh(iq) + l_s q^2 \sinh(iq) & iq \cosh(iq) + \sinh(iq) \\ + l_s [i^2 q^2 \cosh(iq) + 2iq \sinh(iq)] & & + l_s [i^2 q^2 \sinh(iq) + 2iq \cosh(iq)] \end{bmatrix}, \quad (5g)$$

$$\hat{C}_1 = \begin{bmatrix} 0 \\ l_s/2 \\ nl_s/2 \end{bmatrix}, \quad \hat{C}_2 = \begin{bmatrix} 0 \\ \frac{1}{2} g_p^{\perp(1)''}(0) \\ -\frac{n}{2} g_p^{\perp(1)''}(1) \end{bmatrix}. \quad (5h)$$

The constants,  $K_1$  and  $K_2$  are defined as

$$K_1 = -\frac{l_s \{n g_p^{\perp(1)''}(1) + g_p^{\perp(1)''}(0)\}}{s(2l_s + 1)}, \quad (5i)$$

$$K_2 = \frac{1}{2} l_s g_p^{\perp(1)''}(0) + l_s K_1. \quad (5j)$$

Note that if we make  $n = 1$ , the coefficient  $K_1 = 0$ , which makes the net flow velocity in the second order be uniform across the section. The effects of the phase difference angle  $\theta$  is not very clear in the present case, but becomes obvious for the flow driven by the induced electric field. Using the continuity equation (2c) and the boundary condition (3b), one can easily deduce the  $y$ -directional velocity component from the expressions given above.

The volume flow rate contributed by the applied pressure gradient can be calculated from the velocity profiles given in (5a)–(5j) and can be expressed as

$$V_p^\perp = \frac{1}{2} \left( l_s + \frac{1}{6} \right) + \delta^2 \left( \frac{1}{2} K_1 + K_2 \right). \quad (5k)$$

Note that, in expression (5k) the volume flow rate has been nondimensionalized as  $V_p^\perp \rightarrow V_p^\perp / u_{p,\text{ref}} H$ .

## 2. Effect of induced surface potential

The surface potentials on the walls induce an electrostatic field of their own, which dictates the charge distribution in the channel. The induced electrostatic potential ( $\psi$ ) can be described by the Poisson-Boltzmann equation for small values of the surface potential [34–37] with the Debye-Hückel linearization, and is expressed as

$$\nabla^2 \psi = \lambda^2 \psi, \quad (6)$$

where  $\lambda = \sqrt{\frac{2n_0 z^2 e^2}{\epsilon k T}}$  is called the inverse of the Debye length and  $n_0$  is the reference number density of the mobile charges or the bulk fluid ion density. It is important to note that Eq. (1) has been expressed in a nondimensional form and the variables have been nondimensionalized as  $x \rightarrow \frac{x}{H}, y \rightarrow \frac{y}{H}, \psi \rightarrow \frac{\psi}{\zeta_0}, \rho_e \rightarrow \frac{\rho_e}{2\rho_0}, \lambda \rightarrow \lambda H$ , where  $\rho_e$  is the volumetric charge density in the fluid and  $\rho_0$  is the reference charge density. As mentioned earlier, we do not use any separate symbol for the nondimensional variables. The boundary conditions for the potential read

$$\psi(0) = \psi(1) = 1 + m \cos(qx). \quad (7)$$

The solution of Eq. (6), subjected to the boundary condition (7) is given by

$$\psi = \frac{\cosh[\lambda(1/2 - y)]}{\cosh(\lambda/2)} + m \frac{\cosh[Q(1/2 - y)]}{\cosh(Q/2)} \cos(qx). \quad (8)$$

Here,  $Q = \sqrt{\lambda^2 + q^2}$ . The charge density in the solution can be obtained from the Poisson equation, expressed as

$$\rho_e = \beta \psi, \quad \text{where} \quad \beta = -\frac{ze\zeta_0}{kT}. \quad (9)$$

It is important to note here that the electrostatic potential distribution and hence the charge density remains the same, whether the applied pressure gradient is along the  $x$  or the  $z$  axis. Another important point regarding the charge distribution is that Eqs. (6) and (8) are based on the assumption that the effects of advection in the Poisson-Nernst-Planck (PNP) model are negligible and the ions are in local equilibrium. A simple nondimensionalization of the Nernst-Planck equations demonstrates that this assumption remains valid for relatively low values of ionic Peclet numbers [60], defined as  $\text{Pe} = u_{\text{ref}} H / D$

(where  $D$  is the ionic diffusivity). In the present analysis, the largest  $u_{\text{ref}}$  is the one caused by the applied pressure gradient, expressed as  $u_{\text{ref}} \sim H^2 \Omega / \mu$ . Choosing,  $H \sim 10^{-6}$  m,  $\mu \sim 10^{-3}$  Pa s, and  $D \sim 10^{-9}$  m<sup>2</sup>/s (usual values of ionic diffusivity [61]), we get  $\text{Pe} \sim 10^{-6} \Omega$  or less. Hence, for  $\Omega \sim 10^4$ – $10^5$ , we get  $\text{Pe} \sim O(10^{-2})$ , for which the effects of advection can be neglected and the Poisson-Boltzmann description of the ionic distribution remains valid for flows in perpendicular direction. Therefore, in conclusion, the charge distribution assumed in the present analysis remains valid, when  $\Omega \sim 10^4$ – $10^5$  or less and the channel height remains  $H \sim 1$   $\mu\text{m}$  or less. We additionally note that the assumption of equilibrium charge distribution in the PNP model has been employed previously by a number of researchers [35–37,49,50,52,59,60] for analyzing electro-osmotic flows [36,37,49,60] as well as streaming currents [35,50,52,59].

## 3. Velocity distribution due to interactions between the interfacial charges and the induced streaming potential

For the velocity component,  $u_e^\perp$ , due to the induced electric field, the following governing equations (in dimensionless form) hold true:

$$-\frac{\partial p}{\partial x} + \nabla^2 u_e^\perp + \lambda^2 \psi = 0, \quad (10a)$$

$$-\frac{\partial p}{\partial y} + \nabla^2 v_e^\perp = 0, \quad (10b)$$

$$\frac{\partial u_e}{\partial x} + \frac{\partial v_e}{\partial y} = 0. \quad (10c)$$

The nondimensionalization has been done as  $u_e \rightarrow u_e / u_{e,\text{ref}}, v_e \rightarrow v_e / u_{e,\text{ref}}, p \rightarrow p / p_0$ , where  $u_{e,\text{ref}} = -\frac{\epsilon \zeta_0 E_0^\perp}{\mu}$ ,  $p_0 = \frac{\mu u_{e,\text{ref}}}{H}$ , and  $x, y$  have been nondimensionalized in the same way as in Eqs. (2a)–(2c). Note that in Eqs. (10a)–(10c), the pressure gradient is the one induced by virtue of the axial modulations in the slip length as well as the surface potential. The boundary conditions for Eqs. (10a)–(10c) are of same type as given in Eqs. (3a)–(3c). The solutions to Eqs. (10a)–(10c) may be provided in terms of a stream function [34]:

$$\begin{aligned} \phi_e &= (\phi_{e0}^{(0)} + \delta \phi_{e0}^{(1)} + \delta^2 \phi_{e0}^{(2)}) + m (\phi_{e1}^{(0)} + \delta \phi_{e1}^{(1)} + \delta^2 \phi_{e1}^{(2)}), \\ u_e^\perp &= \frac{\partial \phi_e}{\partial y}, \end{aligned} \quad (11a)$$

where

$$\phi_{e0}^{(0)} = \left[ 1 + l_s \lambda \tanh\left(\frac{\lambda}{2}\right) \right] y + \frac{\sinh\left[\lambda\left(\frac{1}{2} - y\right)\right]}{\lambda \cosh\left(\frac{\lambda}{2}\right)}, \quad (11b)$$

$$\phi_{e0}^{(1)} = g_e^1(y) \cos(qx + \theta), \quad (11c)$$

$$\begin{aligned} \phi_{e0}^{(2)} &= \frac{1}{2} G_1 y^2 + G_2 y + \{e_1 y \cosh(qy) + (e_2 + e_3 y) \sinh(qy)\} \\ &\quad \times \cos(2qx + 2\theta), \end{aligned} \quad (11d)$$

$$\phi_{e1}^{(0)} = f_0(y) \cos(qx), \quad (11e)$$

$$\phi_{e1}^{(1)} = \frac{1}{2} K_{e1} y^2 + K_{e2} y + f_1(y) \cos(2qx + \theta), \quad (11f)$$

$$\begin{aligned} \phi_{e0}^{(2)} &= f_2(y) \cos(qx) + f_3(y) \cos(qx + \theta) \\ &\quad + f_4(y) \cos(3qx + 2\theta). \end{aligned} \quad (11g)$$

The functions in the expressions (11c)–(11g) are given by

$$g_1(y) = \{d_1 y \cosh(qy) + (d_2 + d_3 y) \sinh(qy)\}, \quad (11h)$$

$$f_0(y) = (c_0^0 + c_1^0 y) \cosh(qy) + (c_2^0 + c_3^0 y) \sinh(qy) + \frac{Q}{\lambda^2 \cosh(Q/2)} \sinh[Q(1/2 - y)], \quad (11i)$$

$$f_1(y) = c_1^1 y \cosh(2qy) + (c_2^1 + c_3^1 y) \sinh(2qy), \quad (11j)$$

$$f_2(y) = c_1^2 y \cosh(qy) + (c_2^2 + c_3^2 y) \sinh(qy), \quad (11k)$$

$$f_3(y) = c_1^3 y \cosh(qy) + (c_2^3 + c_3^3 y) \sinh(qy), \quad (11l)$$

$$f_4(y) = c_1^4 y \cosh(3qy) + (c_2^4 + c_3^4 y) \sinh(3qy). \quad (11m)$$

The coefficients of the hyperbolic terms are given by

$$\Gamma(1)\hat{d} = \hat{X}_1 \quad \text{and} \quad \Gamma(2)\hat{e} = \hat{X}_2. \quad (11n)$$

The matrices are given by

$$\hat{d}^T = [d_1 \ d_2 \ d_3], \quad \hat{e}^T = [e_1 \ e_2 \ e_3], \quad (11o)$$

$$\hat{X}_1 = \begin{bmatrix} 0 \\ l_s \lambda \tanh(\frac{\lambda}{2}) \\ n l_s \lambda \tanh(\frac{\lambda}{2}) \end{bmatrix}, \quad \hat{X}_2 = \begin{bmatrix} 0 \\ \frac{l_s}{2} g_e^{1''}(0) \\ -\frac{n l_s}{2} g_e^{1''}(1) \end{bmatrix}. \quad (11p)$$

The coefficients  $G_1$  and  $G_2$  are given by

$$G_1 = -\frac{l_s}{2(2l_s + 1)} [n g_e^{1''}(1) + g_e^{1''}(0)], \quad (11q)$$

$$G_2 = \frac{l_s}{2} \left\{ g_e^{1''}(0) \left( 1 - \frac{l_s}{2l_s + 1} \right) - \frac{n l_s g_e^{1''}(1)}{2l_s + 1} \right\}. \quad (11r)$$

The coefficients  $K_1$  and  $K_2$  are given by

$$K_{e1} = \frac{(n-1)l_s f_0''(0) \cos \theta}{2(2l_s + 1)}, \quad (11s)$$

$$K_{e2} = \frac{1}{2} l_s f_0''(0) \cos \theta + l_s K_{e1}, \quad (11t)$$

$$\Gamma(1)\hat{c}^0 = \hat{X}_3, \quad \Gamma(2)\hat{c}^1 = \hat{X}_4, \quad \Gamma(1)\hat{c}^2 = \hat{X}_5, \quad \Gamma(1)\hat{c}^3 = \hat{X}_6, \quad \text{and} \quad \Gamma(3)\hat{c}^4 = \hat{X}_5, \quad (11u)$$

$$c_0^0 = -\frac{Q}{\lambda^2} \tanh\left(\frac{Q}{2}\right), \quad \hat{c}^i = [c_1^i \ c_2^i \ c_3^i], \quad \text{where} \quad i = 0-4, \quad (11v)$$

$$\hat{X}_3 = \begin{bmatrix} \frac{Q}{\lambda^2} \tanh\left(\frac{Q}{2}\right) [1 + \cosh(q)] \\ Q l_s \tanh(Q/2) + \frac{Q^2}{\lambda^2} \\ \frac{Q^2}{\lambda^2} [1 + Q l_s \tanh\left(\frac{Q}{2}\right)] + \frac{q Q}{\lambda^2} \tanh\left(\frac{Q}{2}\right) [l_s q \cosh(q) + \sinh(q)] \end{bmatrix}, \quad (11w)$$

$$\hat{X}_4 = \begin{bmatrix} 0 \\ \frac{1}{2} l_s f_0''(0) \\ -\frac{n}{2} l_s f_0''(1) \end{bmatrix}, \quad (11x)$$

$$\hat{X}_5 = \begin{bmatrix} 0 \\ \frac{1}{2} l_s f_1''(0) \\ -\frac{n}{2} l_s f_1''(1) \end{bmatrix}, \quad \hat{X}_6 = \begin{bmatrix} 0 \\ l_s K_{e1} \\ -n l_s K_{e1} \end{bmatrix}. \quad (11y)$$

$\Gamma(i)$  s can be obtained from the general expression given in Eq. (5c). The volume flow contributed by the electric field can be deduced from the profiles (11a)–(11y), which reads

$$V_e^\perp = 1 + \lambda l_s \tanh\left(\frac{\lambda}{2}\right) - \frac{2 \tanh\left(\frac{\lambda}{2}\right)}{\lambda} + m \delta \left( \frac{1}{2} K_{e1} + K_{e2} \right) + \delta^2 \left( \frac{1}{2} G_1 + G_2 \right). \quad (12)$$

The volume flow rate has been made nondimensional as follows:  $V_e^\perp \rightarrow V_e^\perp / u_{e,\text{ref}} H$ .

#### 4. Streaming potential evaluation

The charge density combined with the fluid velocity imparted by the applied pressure gradient and the induced electric field creates a net transport of charge called the

streaming current. One can obtain the streaming current by simply integrating the product of the velocity and the charge density across the channel. It is obvious that the highly periodic velocity profiles and charge distribution will generate streaming current also periodic in nature, but the important contribution comes from the net components of the streaming currents, which are obtained by taking an average along the axial direction. This is understandable since the streaming potential is the result of net accumulation of charged species in a preferred direction due to the presence of fluid motion. We observe that the periodic components of the streaming current would not result in any net accumulation of the ionic charges in a preferred direction and hence will have no effect on the genesis of the streaming potential. Therefore, the sole effect of streaming current on the streaming potential comes from the net components of the same. Previously, Ajdari [36], Brunet and Ajdari [35], and Zhao [59] have deduced the

streaming current for periodic flows and demonstrated that the net effect comes from the averaged components along the  $x$  direction (axial direction). Ajdari [36] has depicted that for a microchannel with undulated walls under the regime of lubrication approximation, the averaged streaming current from the pressure driven flow and the net throughput from the electric field satisfy the Onsager reciprocity relation, albeit in the limit of thin EDL. Brunet and Ajdari [35] extended the analysis and further demonstrated that the Onsager relation can also be satisfied without the lubrication approximation, for undulated channels with modulated surface charge. In their work the streaming current was again space averaged in the axial direction. Referring back to the present case, streaming current can be expressed in the following form:

$$I_s^\perp = I_p^\perp + I_e^\perp. \quad (13)$$

Here,  $p$  and  $e$  signify the contributions from the pressure gradient and the induced electric field, respectively. The pressure driven streaming current can be expressed in a nondimensional form (nondimensionalized as  $I_p^\perp \rightarrow I_p^\perp / 2\rho_0 u_{p,\text{ref}} H$ ) as

$$I_p^\perp = I_p^{\perp(0)} + \delta I_p^{\perp(1)} + \delta^2 I_p^{\perp(2)} + O(\delta^3), \quad (14a)$$

where

$$I_p^{\perp(0)} = \frac{\beta}{2 \cosh(\lambda/2)} \times \int_0^1 \{y(1-y) + l_s\} \cosh[\lambda(1/2 - y)] dy, \quad (14b)$$

$$I_p^{\perp(1)} = \frac{m\beta Q \cos \theta}{2 \cosh(Q/2)} \int_0^1 g_p^1(y) \sinh[Q(1/2 - y)] dy, \quad (14c)$$

$$I_p^{\perp(2)} = \frac{\beta}{\cosh(\lambda/2)} \int_0^1 (K_1 y + K_2) \cosh[\lambda(1/2 - y)] dy. \quad (14d)$$

It is interesting to note that, because of the periodic components of the velocity generated from the modulated slip on the channel walls, there exists a net component of the streaming current from the periodic part of the surface potential as given in expression (14c), which underlines the effects of the modulated slip in altering the streaming current. The component (14c) is the combined effect of modulated slip and surface charge, whereas the component in Eq. (14d) arises from the combined consequences of modulated slip and the axially invariant part of the surface charge (or, equivalently, the  $\zeta$  potential). Reviewing expression (14c), one can appreciate the effects of the phase difference angle on the streaming current as the contributions from the periodic part of the potential can be completely nullified by rendering  $\theta = \pi/2$  and can be reversed by rendering  $\theta = \pi$ . Thus, it is naturally expected that the effect of modulated slip on the streaming potential in the presence of modulated surface potential would be maximum when the patterned component of the slip and the surface potential are in phase, whereas the same will be minimum when they are out of phase.

It follows from the periodic nature of the streaming current and the velocity profiles that the charges would be carried in and out of the double layer by the periodic streams of

fluid. Therefore, it is important here to check for the total charge conservation in the channel. Referring to the work of Brunet and Ajdari [35], we note that in their study, a thin EDL limit was considered, where all the charges were considered to reside inside a thin surface adhering layer, which produced a streaming current, denoted as the surface current. Brunet and Ajdari demonstrated that because of the presence of periodic variations in the streaming current along with the topographical modulations on the surfaces, the streaming current has a net surface divergence, which spills charge out into the bulk solution from the Debye layer. Therefore, in an effort to conserve the total amount of charge in the Debye layer, an additional potential difference would be induced in the channel, which will direct a current (conduction current) into the Debye layer, maintaining the total amount of charge in the process. The reason behind the genesis of such net component of the divergence of surface current was the presence of topographical undulations on the surfaces and the fact the streaming current was considered only as a surface current, as attributable to the TDL approximation, mathematically realized in the form of Helmholtz-Smoluchowski slip velocity, used as the boundary condition, albeit for the electro-osmotically driven flows. However, in the present analysis, any such topographical undulations are absent, although the streaming current is periodic in nature. Additionally, we have discarded the much used thin EDL approximation and hence we do not have to explicitly account for the presence of any separate layer of charge (or, EDL), where a surface current will be generated by virtue of fluid movement. As a result of this we do not have to account for any additionally induced potential, the sole purpose of which is to send the charges back into the EDL, in order to conserve the total amount of charge. In an effort to delve deeper into such claims we note that the streaming current density from the pressure driven flow can be expressed in the following way (nondimensional, nondimensionalized with  $j_0 = \rho_0 u_{p,\text{ref}}$ ):

$$\mathbf{j}_p = \rho_e \mathbf{v}_p. \quad (15)$$

Referring to Eq. (9), the charge density is given by

$$\rho_e = \beta \psi, \quad \text{where} \quad (16)$$

$$\psi = \frac{\cosh[\lambda(1/2 - y)]}{\cosh(\lambda/2)} + m \frac{\cosh[Q(1/2 - y)]}{\cosh(Q/2)} \cos(qx).$$

Hence, the current density is finally expressed as

$$\mathbf{j}_p = \beta \psi \left[ \{u_p^{(0)} + \delta u_p^{(1)} + \delta^2 u_p^{(2)} + O(\delta^3)\} \mathbf{e}_x + \{\delta v_p^{(1)} + \delta^2 v_p^{(2)} + O(\delta^3)\} \mathbf{e}_y \right]. \quad (17)$$

Here,  $\mathbf{e}_x$  and  $\mathbf{e}_y$  denote unit vectors along the  $x$  and  $y$  axes, respectively. Also note that  $v_p^{(0)} = 0$ . Following Brunet and Ajdari [35], we calculate the total net (averaged over  $x$ ) divergence of the current density in an effort to know whether there is any source of charge consumption or creation. The total net divergence of the current density (in their work Brunet and Ajdari deduced the net surface divergence, since thin EDL was

considered) is given by

$$N = \int_0^{2\pi/q} \int_0^1 \nabla \cdot \mathbf{j}_p dy dx$$

$$= \int_0^{2\pi/q} \int_0^1 \frac{\partial j_{p,x}}{\partial x} dy dx + \int_0^{2\pi/q} \int_0^1 \frac{\partial j_{p,y}}{\partial y} dy dx. \quad (18a)$$

The second term under integration can be simplified as follows:

$$\int_0^{2\pi/q} \int_0^1 \frac{\partial j_{p,y}}{\partial y} dy dx = \int_0^{2\pi/q} [j_{p,y}(1) - j_{p,y}(0)] dx. \quad (18b)$$

Again, we recall that,  $v_p(1) = v_p(0) = 0$  (as attributable to the no penetration boundary condition). Finally, with the help of Eq. (17), (18b) renders to

$$\int_0^{2\pi/q} [j_{p,y}(1) - j_{p,y}(0)] dx = 0. \quad (18c)$$

The first integral in Eq. (18a) can be broken down by order of magnitude in the following way:

$$\frac{\partial j_{p,x}}{\partial x} = \left. \frac{\partial j_{p,x}}{\partial x} \right|^{(0)} + \delta \left. \frac{\partial j_{p,x}}{\partial x} \right|^{(1)} + \delta^2 \left. \frac{\partial j_{p,x}}{\partial x} \right|^{(2)} + O(\delta^3). \quad (19)$$

Here

$$\left. \frac{\partial j_{p,x}}{\partial x} \right|^{(0)} = -q F_{x,0}(y) \sin(qx), \quad (20a)$$

$$F_{x,0}(y) = \frac{m}{2} \{y(1-y) + l_s\} \frac{\cosh[Q(1/2-y)]}{\cosh(Q/2)},$$

$$\left. \frac{\partial j_{p,x}}{\partial x} \right|^{(1)} = -q F_{x,11}(y) \sin(qx + \theta) - 2q F_{x,12}(y) \sin(2qx + \theta), \quad (20b)$$

where

$$F_{x,11} = g_p^{1'}(y) \frac{\cosh[\lambda(1/2-y)]}{\cosh(\lambda/2)},$$

$$F_{x,12} = \frac{m}{2} g_p^{1'}(y) \frac{\cosh[Q(1/2-y)]}{\cosh(Q/2)},$$

$$\left. \frac{\partial j_{p,x}}{\partial x} \right|^{(2)} = -q F_{x,21}(y) \sin(qx) - 2q F_{x,22}(y) \sin(2qx + 2\theta) - F_{x,23}(y) [3q \sin(3qx + 2\theta) + q \sin(qx + 2\theta)], \quad (20c)$$

where

$$F_{x,21}(y) = m(K_1 y + K_2) \frac{\cosh[Q(1/2-y)]}{\cosh(Q/2)},$$

$$F_{x,22}(y) = g_p^{2'}(y) \frac{\cosh[\lambda(1/2-y)]}{\cosh(\lambda/2)},$$

$$F_{x,23} = \frac{m}{2} g_p^{2'}(y) \frac{\cosh[Q(1/2-y)]}{\cosh(Q/2)}.$$

A close review of Eqs. (19) and (20) reveals that the left-hand side in Eq. (19), i.e., the term under integration, is completely periodic in  $x$  and hence averaging the same along the  $x$  direction would result in net zero value; i.e.,

$$\int_0^{2\pi/q} \int_0^1 \frac{\partial j_{p,x}}{\partial x} dy dx = 0. \quad (21)$$

Therefore, the net total divergence of the streaming current density turns out to be zero ( $N = 0$ ). It thus follows from the work of Brunet and Ajdari [35] that there will not be any additionally induced potential, since there is no net creation or consumption of charges (or, in other words no net spilling of charges out of the EDLs). This is understandable since in the present case we have not considered topographical undulations in the channel walls and hence the net divergence becomes zero, as was also the case in the analysis previously executed by Brunet and Ajdari [35]. The same approach has also been adapted by Zhao [59], while evaluating the streaming potential for surfaces with patterned wettability, albeit for an unbounded domain restricted only by a bottom wall. In that study, the streaming potential was considered to be a constant (i.e., independent of  $x$ ) and the streaming currents were determined by averaging the cross sectional charge throughput.

The contribution of the electric field on the streaming current can also be calculated in a similar fashion and can be expressed in a nondimensional form (nondimensionalized as  $I_e^\perp \rightarrow I_e^\perp / 2\rho_0 u_{e,\text{ref}} H$ ) as follows:

$$I_e^\perp = I_e^{\perp(0)} + \delta I_e^{\perp(1)} + \delta^2 I_e^{\perp(2)} + O(\delta^3), \quad (22a)$$

$$I_e^{\perp(0)} = \frac{\beta}{\cosh(\lambda/2)} \times \int_0^1 \left\{ 1 + l_s \tanh(\lambda/2) - \frac{\cosh[\lambda(1/2-y)]}{\cosh(\lambda/2)} \right\} \times \cosh[\lambda(1/2-y)] dy + \frac{m^2 \beta Q}{2 \cosh(Q/2)} \int_0^1 f_0(y) \sinh[Q(1/2-y)] dy, \quad (22b)$$

$$I_e^{\perp(1)} = \frac{m\beta}{\cosh(\lambda/2)} \int_0^1 (K_{e1} y + K_{e2}) \cosh[\lambda(1/2-y)] dy + \frac{m\beta Q \cos \theta}{2 \cosh(Q/2)} \int_0^1 g_e^{1'}(y) \sinh[Q(1/2-y)] dy, \quad (22c)$$

$$I_e^{\perp(2)} = \frac{\beta}{\cosh(\lambda/2)} \int_0^1 (G_1 y + G_2) \cosh[\lambda(1/2-y)] dy + \frac{m^2 \beta Q}{2 \cosh(Q/2)} \int_0^1 \{f_2(y) + f_3(y) \cos \theta\} \times \sinh[Q(1/2-y)] dy. \quad (22d)$$

It should be mentioned that, for low surface potentials, the streaming current for the electric field becomes negligible as compared to the streaming current contributed from the applied pressure gradient. Nevertheless, one interesting thing to note from the expressions (22b)–(22d) is that the combined effects of the modulated slip as well as modulated potential appears in all three components, unlike the streaming current generated by virtue of pressure driven flow. However, the effect of the

phase difference appears only in Eqs. (22c) and (22d) and again the effects of the modulated and axially invariant components of the surface potential can be manipulated to aid and oppose each other by making  $\theta = 0$  and  $\pi$ , respectively.

At this stage we can calculate the induced streaming potential by invoking the electro-neutrality criterion, which states that the net current through the channel should be zero if no external electric field is applied [1,5]. This can be expressed mathematically as

$$2\rho_0 u_{p,\text{ref}} H I_p^\perp - \frac{2\rho_0 \varepsilon \zeta_0 E_0^\perp H}{\mu} I_e^\perp + I_c^\perp = 0. \quad (23)$$

In Eq. (23),  $I_c^\perp$  denotes the conduction current generated from the induced electric field. The conduction current can be expressed as a function of the electrical conductivity of the solution in the presence of low surface potential, which takes the form

$$I_c^\perp = \sigma H E_0^\perp, \quad \sigma = \frac{2n_0 z^2 e^2}{f}. \quad (24)$$

Here,  $f$  is the friction factor for the ions moving inside the fluid and  $\sigma$  is the electrical conductivity of the solution. Strictly speaking, the conductivity is a strong function of the ion concentrations and, hence, the EDL potential distribution. The conductivity ( $\sigma/\sigma_0$ ;  $\sigma_0 = 2n_0 z^2 e^2/f$ ) comes out to be  $O[\cosh(\psi)]$ , which on expanding becomes  $\frac{\sigma}{\sigma_0} \approx 1 + \frac{\psi^2}{2} + O(\psi^4)$ . For low surface potential, one can neglect the  $\psi^2$  terms and can approximate the conductivity to be  $\sigma_0$ . One can obtain a solution for the induced electric field  $E_0$ , by solving Eq. (23), by replacing the conduction current with expression (24), which takes the following form:

$$E_0^\perp = -\frac{I_p^\perp}{\gamma - \alpha_1 I_e^\perp} \Omega^\perp. \quad (25)$$

In expression (25),  $\gamma = \frac{ze\mu}{H^2 f}$ ,  $\alpha_1 = \frac{\varepsilon \zeta_0}{H^2}$ . Equivalently, Eq. (25) can be written as  $E_0^\perp = R^\perp \Omega^\perp$ , where,  $R^\perp = -\frac{I_p^\perp}{\gamma - \alpha_1 I_e^\perp}$ .

## B. Applied pressure gradient in the $z$ (parallel) direction

### 1. Pressure driven flow

A pressure gradient of magnitude  $\Omega^\parallel$  along the  $z$  direction in the channel is applied in order to actuate the flow, which induces a streaming potential mathematically denoted by  $E_0^\parallel$ . The equation, combining the effects of the induced electric field is given by

$$-\frac{dp}{dz} + \mu \nabla^2 w^\parallel + \rho_e E_0^\parallel = 0. \quad (26)$$

One can separate solutions for pressure driven and electro-osmotically driven flows ( $w^\parallel = w_p^\parallel + w_e^\parallel$ ) in a way similar to that in the previous section. Implementing the same nondimensionalization scheme as discussed in Sec. II A 1, one can obtain the equations for the pressure driven flow as

$$-\frac{dp}{dz} + \nabla^2 w_p^\parallel = 0. \quad (27)$$

Note that here  $w_{p,\text{ref}} = \frac{H^2 \Omega^\parallel}{\mu}$ . Boundary conditions for  $w$  remain the same as conditions (3a), with  $u^\perp$  replaced with  $w^\parallel$ . A solution of the form (4) can be obtained for  $w^\parallel$ , which can be written as

$$w_p^\parallel = w_p^{\parallel(0)} + \delta w_p^{\parallel(1)} + \delta^2 w_p^{\parallel(2)} + O(\delta^3). \quad (28)$$

Here

$$w_p^{\parallel(0)} = \frac{1}{2} \{y(1-y) + l_s\}, \quad (29a)$$

$$w_p^{\parallel(1)} = h_{p1}(y) \cos(qx + \theta), \quad (29b)$$

$$h_{p1}(y) = [b_{p11} \cosh(qy) + b_{p12} \sinh(qy)],$$

where

$$b_{p12} = \frac{l_s [n - s_1(q)]}{2s_2(q)}, \quad b_{p11} = \frac{1}{2} l_s + l_s q b_{p12},$$

$$w_p^{\parallel(2)} = \chi_1 y + \chi_2 + [b_{p21} \cosh(2qy) + b_{p22} \sinh(2qy)] \times \cos(2qx + 2\theta), \quad (29c)$$

where

$$\chi_1 = -\frac{q l_s}{2(2l_s + 1)} \{n b_{p11} \sinh(q) + b_{p12} [n \cosh(q) + 1]\}$$

and

$$\chi_2 = \frac{1}{2} l_s q b_{p12} + l_s \chi_1, \quad (29d)$$

$$b_{p22} = -\frac{n l_s h'_{p1}(1) + l_s h'_{p1}(0) s_1(2q)}{2s_2(2q)},$$

$$b_{p21} = \frac{1}{2} l_s + 2l_s q b_{p22}.$$

In Eqs. (22a)–(22d),

$$s_1(iq) = \cosh(iq) + i q l_s \sinh(iq)$$

and

$$s_2(iq) = (1 + i^2 q^2 l_s^2) \sinh(iq) + 2i q l_s \cosh(iq). \quad (29e)$$

Note that the “dash” sign on the various functions denotes derivative with respect to  $y$ . The volume flow rate can be obtained from the velocity profiles:

$$V_p^\parallel = \frac{1}{2} \left( l_s + \frac{1}{6} \right) + \delta^2 \left( \frac{1}{2} \chi_1 + \chi_2 \right). \quad (30)$$

### 2. Velocity distribution for induced streaming potential

For the velocity component,  $w_e^\parallel$ , due to the induced electric field, the following governing equations (in dimensionless form) hold true:

$$\nabla^2 w_e^\parallel + \lambda^2 \psi = 0. \quad (31)$$

Equation (24) has been obtained for the charge distribution given in Eq. (9). The solution to Eq. (24) takes the same form as given in Eq. (4) and can be expressed as

$$w_e^\parallel = (w_{e0}^{\parallel(0)} + \delta w_{e0}^{\parallel(1)} + \delta^2 w_{e0}^{\parallel(2)}) + m (w_{e1}^{\parallel(0)} + \delta w_{e1}^{\parallel(1)} + \delta^2 w_{e1}^{\parallel(2)}) + O(\delta^3). \quad (32)$$

Note that, subscript 0 denotes contribution from the axially invariant part of the surface potential and subscript 1 denotes

that from the axially varying component. The individual contributions can be expressed as

$$w_{e0}^{\parallel(0)} = \left[ 1 + l_s \lambda \tanh\left(\frac{\lambda}{2}\right) \right] - \frac{\cosh\left[\lambda\left(\frac{1}{2} - y\right)\right]}{\lambda \cosh\left(\frac{\lambda}{2}\right)}, \quad (33a)$$

$$w_{e0}^{\parallel(1)} = h_{e01}(y) \cos(qx + \theta), \quad (33b)$$

where

$$h_{e01}(y) = \kappa_{11} \cosh(qy) + \kappa_{12} \sinh(qy),$$

with

$$\kappa_{11} = \frac{l_s \lambda \tanh(\lambda/2)[s_3(q) - nl_s q]}{s_2(q)}$$

and

$$\kappa_{12} = \frac{\kappa_{11} - \lambda l_s \tanh(\lambda/2)}{l_s q}, \quad (33c)$$

$$w_{e0}^{\parallel(2)} = \eta_1 y + \eta_2 + h_{e02}(y) \cos(2qx + 2\theta),$$

where

$$h_{e01}(y) = \kappa_{21} \cosh(2qy) + \kappa_{22} \sinh(2qy),$$

where

$$\eta_1 = -\frac{l_s [nh'_{e01}(1) + h'_{e01}(0)]}{2(2l_s + 1)}$$

and

$$\eta_2 = \frac{1}{2} h'_{e01}(0) + l_s \eta_1, \text{ with}$$

$$\kappa_{21} = \frac{l_s [h'_{e01}(0)s_3(2q) - 2nl_s q h'_{e01}(1)]}{2s_2(2q)}$$

and

$$\kappa_{22} = \frac{\kappa_{21} - (1/2)l_s h'_{e01}(0)}{2l_s q}.$$

The contributions from the axially varying part of the surface potential are given by

$$w_{e1}^{\parallel(0)} = h_{e10}(y) \cos(qx),$$

$$h_{e10}(y) = k_{01} \cosh(qy) + k_{02} \sinh(qy) - \frac{\cosh[Q(1/2 - y)]}{\cosh(Q/2)}, \quad (33d)$$

where

$$k_{01} = \frac{[l_s Q \tanh(Q/2) + 1][s_3(q) + nl_s q]}{s_2(q)}$$

and

$$k_{02} = \frac{[l_s Q \tanh(Q/2) + 1][-s_1(q) + 1]}{s_2(q)},$$

$$w_{e1}^{\parallel(1)} = \Gamma_1 y + \Gamma_2 + h_{e11}(y) \cos(2qx + \theta), \quad (33e)$$

$$h_{e11}(y) = k_{11} \cosh(2qy) + k_{12} \sinh(2qy),$$

where

$$\Gamma_1 = \frac{l_s \cos(\theta)[nh'_{e1}(1) + h'_{e1}(0)]}{2(2l_s + 1)}$$

and

$$\Gamma_2 = \frac{1}{2} l_s h'_{e1}(0) \cos(\theta) + l_s \Gamma_1,$$

with

$$k_{11} = \frac{l_s q k_{02}[s_3(2q) - 2ql_s n]}{2s_2(2q)}$$

and

$$k_{12} = \frac{k_{11} - (1/2)l_s h'_{e10}(0)}{2l_s q},$$

$$w_{e1}^{\parallel(2)} = h_{e12}(y) \cos(qx + \theta) + h_{e13}(y) \cos(qx) + h_{e14}(y) \cos(3qx + 2\theta), \quad (33f)$$

$$h_{e12}(y) = k_{21} \cosh(qy) + k_{22} \sinh(qy), \quad (33g)$$

$$h_{e13}(y) = k_{31} \cosh(qy) + k_{32} \sinh(qy),$$

$$h_{e14}(y) = k_{41} \cosh(3qy) + k_{42} \sinh(3qy), \quad (33h)$$

where the coefficients are given by

$$k_{21} = \frac{l_s \Gamma_1 [s_3(q) - nl_s q]}{s_2(q)},$$

$$k_{22} = \frac{k_{21} - (1/2)l_s \Gamma_1}{2l_s q},$$

$$k_{31} = \frac{l_s [h'_{e1}(0)s_3(q) - nl_s q h'_{e1}(1)]}{2s_2(q)},$$

$$k_{32} = \frac{k_{31} - (1/2)l_s h'_{e1}(0)}{2l_s q},$$

$$k_{41} = \frac{l_s [h'_{e1}(0)s_3(3q) - 3nl_s q h'_{e1}(1)]}{2s_2(3q)},$$

$$k_{42} = \frac{k_{41} - (1/2)l_s h'_{e1}(0)}{3l_s q}.$$

Here  $s_3(iq) = \sinh(iq) + iq l_s \cosh(iq)$ . The volume flow rate for the electro-osmotic flow can also be calculated easily by integrating the profile and can be expressed as

$$V_e^{\parallel} = 1 + \lambda l_s \tanh\left(\frac{\lambda}{2}\right) - \frac{2 \tanh\left(\frac{\lambda}{2}\right)}{\lambda} + m \delta \left( \frac{1}{2} \Gamma_1 + \Gamma_2 \right) + \delta^2 \left( \frac{1}{2} \eta_1 + \eta_2 \right). \quad (34)$$

### 3. Streaming potential evaluation

Streaming potential for the applied pressure gradient in the  $z$  direction can also be calculated in the same way as in Sec. II A 4. The streaming current is expressed in the same form as in Eq. (13). We calculate the streaming current for the pressure driven flow to be

$$I_p^{\parallel} = I_p^{\parallel(0)} + \delta I_p^{\parallel(1)} + \delta^2 I_p^{\parallel(2)} + O(\delta^3). \quad (35)$$

In Eq. (28) contributions from various orders are given by

$$I_p^{\parallel(0)} = \frac{\beta}{2 \cosh(\lambda/2)} \int_0^1 \{y(1-y) + l_s\} \cosh[\lambda(1/2 - y)] dy, \quad (36a)$$

$$I_p^{\parallel(1)} = \frac{m\beta \cos(\theta)}{2 \cosh(Q/2)} \int_0^1 h_{p1}(y) \cosh[Q(1/2 - y)] dy, \quad (36b)$$

$$I_p^{\parallel(2)} = \frac{\beta}{\cosh(\lambda/2)} \int_0^1 \{\chi_1 y + \chi_2\} \cosh[\lambda(1/2 - y)] dy. \quad (36c)$$

A comparison between Eqs. (36a)–(36c) and (14b)–(14d) reveals that the streaming current in both the directions show the same kind of variation with the phase shift angle and the amplitude of the axially varying component of the surface potential. The only difference between the flows in the  $x$  and the  $z$  directions is that for the present case of flow the  $y$  component of the velocity is absent. Note that Eqs. (36a)–(36c) have been expressed with nondimensional variables, the nondimensionalization scheme being the same for Eqs. (14a)–(14d). Following Eqs. (22a)–(22d), one can evaluate the contribution of the streaming electric field in the total streaming current and the same can be expressed for the flow presently under consideration as

$$I_e^{\parallel} = I_e^{\parallel(0)} + \delta I_e^{\parallel(1)} + \delta^2 I_e^{\parallel(2)} + O(\delta^3). \quad (37)$$

The individual components are given by

$$I_e^{\parallel(0)} = \frac{\beta}{\cosh(\lambda/2)} \int_0^1 \left\{ 1 + I_s \tanh(\lambda/2) - \frac{\cosh[\lambda(1/2 - y)]}{\cosh(\lambda/2)} \right\} \cosh[\lambda(1/2 - y)] dy + \frac{m^2 \beta Q}{2 \cosh(Q/2)} \int_0^1 h_{e10}(y) \cosh[Q(1/2 - y)] dy, \quad (38a)$$

$$I_e^{\parallel(1)} = \frac{m\beta}{\cosh(\lambda/2)} \int_0^1 (\Gamma_1 y + \Gamma_2) \cosh[\lambda(1/2 - y)] dy + \frac{m\beta Q \cos \theta}{2 \cosh(Q/2)} \int_0^1 h_{e01}(y) \cosh[Q(1/2 - y)] dy, \quad (38b)$$

$$I_e^{\parallel(2)} = \frac{\beta}{\cosh(\lambda/2)} \int_0^1 (\eta_1 y + \eta_2) \cosh[\lambda(1/2 - y)] dy + \frac{m^2 \beta Q}{2 \cosh(Q/2)} \int_0^1 \{h_{e12}(y) + h_{e13}(y) \cos \theta\} \times \cosh[Q(1/2 - y)] dy. \quad (38c)$$

Finally applying the assumption of zero net current, one can find out the equation for the streaming potential in the same form as given in Eq. (23):

$$2\rho_0 u_{p,\text{ref}} H I_p^{\parallel} - \frac{2\rho_0 \varepsilon \xi_0 E_0^{\parallel} H}{\mu} I_e^{\parallel} + I_c^{\parallel} = 0. \quad (39)$$

In Eq. (39), the conduction current  $I_c^{\parallel}$  is given by

$$I_c^{\parallel} = \sigma H E_0^{\parallel}. \quad (40)$$

One can express the streaming potential as

$$E_0^{\parallel} = R^{\parallel} \Omega^{\parallel}, \quad \text{where} \quad R^{\parallel} = -\frac{I_p^{\parallel}}{\gamma - \alpha_1 I_e^{\parallel}}. \quad (41)$$

### C. Anisotropic streaming potential for applied pressure gradient in any general direction

In the previous sections we have determined the streaming potential for applied pressure gradients in orthogonal directions. Now we attempt to work out the induced potential for an applied pressure gradient in any direction, which, in

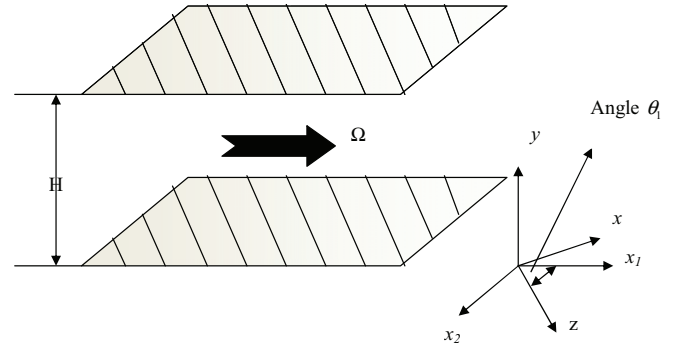


FIG. 1. (Color online) A schematic of the channel with two plates at  $y = 0$  and  $H$ , along with the surface modulations. The direction of the modulation has been shown with the single lines on the plates. Along these lines the values of  $\cos(qx + \theta)$  in the slip modulation is 0. The modulations in the surface potential have not been explicitly shown, as they run parallel to the slip modulations, with a phase shift of  $\theta$ . The orthogonal directions are  $x$  (perpendicular) and  $z$  (parallel), which run along and across the modulations, respectively. The pressure gradient ( $\Omega$ ) has been applied along the  $x_1$  axis, which makes an angle  $\theta_1$  with the  $z$  axis.

general, does not match with the two orthogonal directions. For a better physical outlook we present a schematic of the channel in Fig. 1. The channel height and the other relevant characteristics of modulations remain essentially the same as described earlier. The two orthogonal directions, i.e., the directions parallel and perpendicular to the wettability and charge modulations are denoted by the  $z$  and  $x$  axes, respectively. The applied pressure gradient (magnitude  $\Omega$ ) is assumed to make an angle  $\theta_1$  with the  $z$  axis. We also define a new axis system, with respect to the applied pressure gradient, where the pressure gradient works along the  $x_1$  axis, the  $y$  axis is the same as that of the orthogonal axes system, and  $x_2$  is a mutually perpendicular axis to both  $x_1$  and  $y$ . The induced streaming potential can be expressed in a general form given by

$$\mathbf{E}_0 = E_{0,1} \mathbf{e}_1 + E_{0,2} \mathbf{e}_2, \quad (42)$$

where,  $\mathbf{e}_i$  and  $E_{0,i}$  are unit vectors and induced streaming potential along the  $x_i$  direction, respectively. The two components for the streaming potential can be related to the applied pressure gradient through the following general tensorial relation:

$$\tilde{E} = \tilde{M}^T [\tilde{R} (\tilde{M} \tilde{\Omega})]. \quad (43)$$

The tensors are expressed as

$$\tilde{E} = \begin{bmatrix} E_{0,1} \\ E_{0,2} \end{bmatrix}, \quad \tilde{\Omega} = \begin{bmatrix} \Omega_1 \\ \Omega_2 \end{bmatrix}, \quad \tilde{R} = \begin{bmatrix} R^\perp & 0 \\ 0 & R^\parallel \end{bmatrix}, \quad \text{and} \\ \tilde{M} = \begin{bmatrix} \sin(\theta_1) & -\cos(\theta_1) \\ \cos(\theta_1) & \sin(\theta_1) \end{bmatrix}. \quad (44)$$

In Eqs. (44),  $\Omega_1$  and  $\Omega_2$  denote applied pressure gradients along the  $x_1$  and  $x_2$  directions, respectively. For the present considerations, we note that  $\Omega_1 = \Omega$  and  $\Omega_2 = 0$ . Reviewing Eqs. (41) and (25), one can infer that, in general,  $R^\perp \neq R^\parallel$ , which indicates that an applied pressure gradient along the  $x_1$  direction will generate an induced potential along the  $x_2$  direction, or there will be off-diagonal effects. Denoting the

angle between the streaming potential and the applied pressure gradient (i.e., the  $x_1$  axis) by  $\theta_d$ , we obtain an expression for the same:

$$\theta_d = \tan^{-1} \left[ \tan(\theta_1) \frac{R^\perp}{R^\parallel} \right] - \theta_1. \quad (45)$$

We call this angle the deviation angle. It can be easily verified from Eq. (45) that, by putting  $\theta_1 = 0$  or  $\pi/2$ , i.e., for applied pressure gradients along the orthogonal directions,  $\theta_d = 0$ , which indicates absence of any off-diagonal effects. It can also be observed that a weak anisotropy appears even if there is no wettability modulation present, as attributable to the modulated surface charge, which influences the streaming potential through Eqs. (22a)–(22d) and (38a)–(38c). Differentiating (45), with respect to  $\theta_1$ , one can show that the maximum deviation angle is achieved if  $\theta_1 = \pi/4$ . Following the expressions for the streaming potentials, it becomes apparent that the primary source of anisotropy is the  $O(\delta)$  terms in the streaming current, as the zeroth order streaming currents for pressure driven velocity are identical and the contributions from the  $O(\delta^2)$  terms have significantly smaller effects as compared to the zeroth order terms. Noting that the  $O(\delta)$  terms in Eqs. (14c) and (36b) are outcomes of axially varying components of surface potential, it follows that anisotropy and off-diagonal effects in the induced potential become more prominent for the presence of axially varying surface potential, although the streaming potential achieves higher value for an axially invariant potential. Quite intuitively, it also follows that a higher value of  $\delta$  would result in higher anisotropy and off-diagonal effects.

#### D. Cases of channels with sidewalls along with anisotropic slip and potential modulation

In the previous section, we have considered a channel, open in both the  $x_2$  and the  $x_1$  directions (as depicted in Fig. 1) and have shown that anisotropic streaming potential is generated as a result of such arrangements. However, in practice any channel would consist of sidewalls. Therefore, for practical relevance it is important to investigate the effects of the presence of sidewalls on the induced streaming potential and the resulting anisotropy. In the present section, we consider the same channel as shown in Fig. 1, only closed along the  $x_2$  direction by sidewalls.

As depicted in previous studies [62], the anisotropic patterning tends to create an off-diagonal component of the flow rate. However, the presence of sidewalls will prevent any such flow from occurring. This is achieved through an additionally induced pressure gradient along the lateral direction (between the two side walls), which drives its own fluid currents in order to render the net flow rate along the lateral direction to zero. It has already been shown by Stroock *et al.* [60] that the streamlines take spiral shape in cases of grooved channels, with the grooves being at some angle with the channel axes, i.e., the direction of the applied pressure gradient. However, in the present case, the induced pressure in the transverse direction will again induce a separate streaming potential of its own, which will act in tandem with the one induced by the externally applied pressure gradient. This is quite interesting since the final outcome of these two separate

electric fields is that the direction of the resultant streaming potential will again be somewhat shifted from the direction of the applied pressure gradient, although the net throughput will strictly follow the direction of the applied pressure gradient. This simply indicates that there will be a transverse component of the induced electric field as well. The existence of such transverse components of induced potential in anisotropically patterned channels has already been demonstrated by Ajdari [36], for topographical undulations on the surfaces. In an effort to quantify the aforementioned transverse pressure gradient and the resulting change in the streaming potential, we consider a channel closed along the  $x_2$  direction and an external pressure gradient ( $\Omega_1$ ) has been applied in the same along the  $x_1$  axis (refer to Fig. 1; the channel is of same shape, only closed along the  $x_2$  axis). We first note that the net throughput in a channel with the present form of patterning can be expressed in a tensorial form in the following way:

$$\tilde{J} = u_{\text{ref}} H \tilde{M}^T [\tilde{V}(\tilde{M}\tilde{\Omega})]. \quad (46a)$$

The pressure and the rotation matrices have already been described in Eqs. (44). The additional matrices are given by

$$\tilde{J} = [J_1 \ J_2]^T \quad \text{and} \quad \tilde{V} = \begin{bmatrix} V_p^\perp & 0 \\ 0 & V_p^\parallel \end{bmatrix}. \quad (46b)$$

Here  $J_1$  and  $J_2$  represent net throughputs in the  $x_1$  and  $x_2$  directions (refer to Fig. 1) and the terms  $V_p^\perp$  and  $V_p^\parallel$  have already been derived in Eqs. (5k) and (30), respectively. Note that in equation (46a) the pressure matrix includes the applied as well as the (net) induced pressure gradients. Now, following Ajdari [35], we can find the induced pressure gradient in the  $x_2$  direction by equating  $J_2$  to 0. A simple expansion of the matrices in Eqs. (46a) gives

$$\Omega_2 = \frac{\Omega_1 (V_p^\perp - V_p^\parallel) \sin(\theta_1) \cos(\theta_1)}{V_p^\perp \cos^2 \theta_1 + V_p^\parallel \sin^2 \theta_1}. \quad (47)$$

Note that, in deriving Eqs. (46a) and (47), we have assumed that  $V_E \ll V_p$ ; i.e., the contribution from the streaming potential in modifying the net throughput is small compared to that from the active pressure gradient. Equation (47) shows that there exists a transverse induced pressure gradient when  $V_p^\perp \neq V_p^\parallel$ . We further note that, for  $\theta_1 = 0^\circ$  or  $90^\circ$ , i.e., when the channel axes and the principle axes of the patterning coincide, this induced pressure becomes zero, as expected. Since the pressure gradient in the transverse direction is now known [from Eq. (47)], we can easily calculate the resulting induced streaming potential from the relation [Eq. (43)]:

$$\tilde{E} = \tilde{M}^T [\tilde{R}(\tilde{M}\tilde{\Omega})]. \quad (48)$$

The relevant matrices have already been defined. Therefore, the final result is that a component of the induced potential is present in the transverse direction as well, as evident from Eq. (48). Interestingly, this means, as mentioned earlier, that the net electric field is somewhat shifted from the direction of the applied pressure gradient. This angle shift can be quite easily calculated and turns out to be

$$\theta_S = \tan^{-1} \left( \frac{E_{0,2}}{E_{0,1}} \right). \quad (49)$$

It is clear from Eq. (49) that the present deviation angle and the one defined in Eq. (45) are not the same, since the present one is generated in a channel, which is closed sideways. However, we also note that the genesis of both the deviation angles is the same, i.e., the anisotropy in the flow as attributable to the charge and slip modulations on the surfaces and they essentially reveal the same physics at play. Therefore, it would be enough to investigate any one of them in an effort to deduce the extent of anisotropy. In the present study we do not explicitly seek to investigate the variation in angle  $\theta_S$  and attempt to stick to  $\theta_d$  throughout.

### III. RESULTS AND DISCUSSIONS

In this section, we attempt to pinpoint the effects of the prescribed modulations in surface potential and the surface wettability in particular (represented here as modulated slip on the surfaces) on the corresponding induced streaming potential field and the deviation angle. Towards this, we shall sort out the important parameters that dictate the essential modulation characteristics, especially the modulated slip on the surface. Following the analysis presented in the previous section, we mention the following parameters having major influence on the modulation characteristics and the induced potential: channel height to Debye length ratio ( $\lambda$ ), patterning frequency ( $q$ ), amplitude of wettability modulation ( $\delta$ ), phase difference between the applied slip and the surface potential ( $\theta$ ), and the asymmetry factor ( $n$ ). It is also important to mention here that while the results are calculated on the basis of dimensionless parameters, we ensure that the corresponding dimensional parameters are within the ranges of interest for microfluidic transport with liquid water as the flow medium. It is further important to mention in this context that the value of  $\zeta_0$  in the present analysis is restricted by the choice of the parameter  $m$  so as to ensure the validity of the Debye-Hückel linearization, which holds for surface potential values less than 25 mV.

#### A. Comparison with numerical estimations

In an effort to verify the extent of validity of the perturbation analysis adapted herein, we attempt to solve the corresponding equations numerically to evaluate the resulting streaming potential and match them with our analytical results. Toward this, we first recall the expression for the streaming potential in Eq. (18a) and note that the contribution from the streaming current generated from the induced field (denoted by  $I_e$  in the expression under consideration) is quite small as compared to the contributions from the streaming current from the pressure driven flow ( $I_p$ ) and the conduction current generated from the streaming electric field, for low surface potentials, lying within Debye-Hückel limit. To validate such propositions, we note that the contribution from  $I_e$  is determined by the ratio  $\alpha_1/\gamma$ , which is  $\varepsilon\zeta f/ze\mu$ . For typical values of fluid properties and  $\zeta$  potential values chosen in the present study ( $\zeta \sim 10\text{--}25$  mV,  $f \sim 10^{-12}$ ), this ratio turns out to be  $\sim 10^{-2}\text{--}0.1$ . In the same spirit we also note that the velocity generated from an applied pressure gradient is on the order of  $u_{\text{ref},p} \sim H^2\Omega/\mu$ , where as the same from an electric field turns out to be in the tune of  $u_{\text{ref},e} \sim \varepsilon\zeta E_0/\mu$ . The ratio of the two is given by  $R = u_{\text{ref},e}/u_{\text{ref},p} \sim \varepsilon\zeta E_0/H^2\Omega$ . For the preset sub-section,

we have chosen the following values:  $\varepsilon \sim 6 \times 10^{-10}$ ,  $\zeta \sim 1 - 2 \times 10^{-2}$ ,  $H \sim 10^{-5}$ , and  $E_0/\Omega \sim 10^{-3} - 10^{-4}$  (as can be verified from the analytical results and a simple calculation for a unidirectional flow). Hence, the ratio turns out to be  $R \sim 10^{-4} - 10^{-5} \ll 1$ , which shows that the velocity generated from electric field is much smaller as compared to the pressure gradient. Therefore, in the present section we neglect the contribution from  $I_e$  by dropping the electrical body force term in the momentum equation while calculating the streaming potential, for ease of computation. In fact, such assumptions have already been employed previously by a number of researchers [35,59]. The final momentum balance equation can then be expressed in a nondimensional form as follows:

$$\text{Re} \frac{Du}{Dt} = -\frac{\partial p}{\partial x} + \nabla^2 u, \quad (50a)$$

$$\text{Re} \frac{Dv}{Dt} = -\frac{\partial p}{\partial y} + \nabla^2 v. \quad (50b)$$

The nondimensionalization has been done using the same scheme adapted in Eqs. (2a)–(2c). Here, Re is the Reynolds number, expressed as  $\text{Re} = \frac{\rho u_{\text{ref},p} H}{\mu}$ . Note that, although these equations are not exactly the same with Eqs. (1), the effect of the left-hand side can be nullified by making the Reynolds number very small. Additionally, in Eq. (50a),  $-\frac{\partial p}{\partial x}$  includes externally applied as well as induced pressure gradient. The boundary conditions used to solve Eqs. (50) are same as in Eqs. (3a) and (3b). However, for the sake completeness, we again mention the boundary conditions:

$$u_p^\perp(0) = l_s[1 + \delta \cos(qx + \theta)] \frac{\partial u_p^\perp(y=0)}{\partial y}$$

and

$$u_p^\perp(1) = -l_s[1 + n\delta \cos(qx + \theta)] \frac{\partial u_p^\perp(y=1)}{\partial y}, \quad (3a)$$

$$v_p^\perp(0) = 0, \quad \text{and} \quad v_p^\perp(1) = 0. \quad (3b)$$

Equations (50) are solved numerically using the boundary conditions (3) to obtain the velocity profiles. We have used the commercial software package FLUENT in order to solve the corresponding equations by employing a control volume based finite difference method. The domain for the numerical simulation was taken to be of the size  $H = 1$  and  $L = 2$ . The domain was discretized into  $100 \times 100$  equally sized computational cells. We have used  $\text{Re} = 0.001$ , in an effort to make the effect of inertia negligible as assumed in the analytical solutions. The net streaming current was calculated by averaging the total cross-sectional charge throughput in the following way:

$$I_p = \frac{1}{L} \int_0^L \int_0^H \rho_e u dy dx. \quad (51)$$

The charge density is given by the expression (9):

$$\rho_e = \beta \psi, \quad \text{where} \quad \beta = -\frac{ze\zeta_0}{kT}. \quad (9)$$

Following Eqs. (13) and (23) we evaluate the streaming potential to be (note that  $I_e$  has been neglected, as mentioned

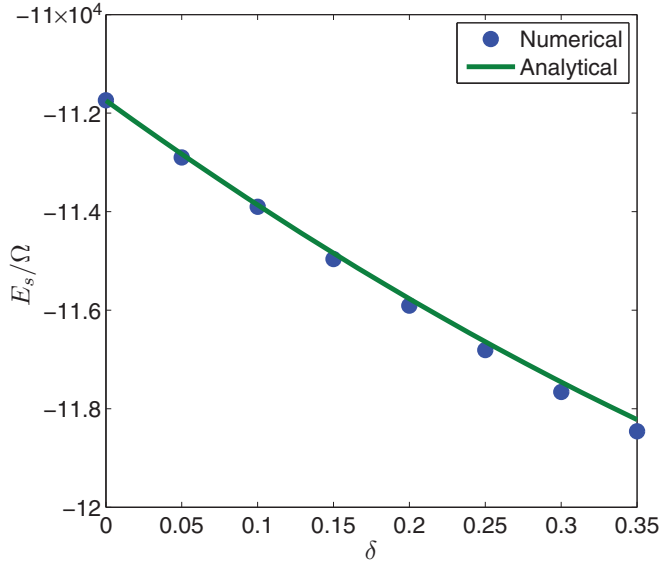


FIG. 2. (Color online) Comparison of analytical and numerical results for evaluation of streaming potential. Analytical (green line) and numerical (blue dots) results for  $E_s/\Omega$  vs  $\delta$  have been plotted in the present figure. The other parameters have been taken as  $n = 1$ ,  $m = 1$ ,  $\theta = 0$ ,  $l_s = 0.05$ ,  $H = 10^{-5}$  m,  $\zeta_0 = 25$  mV,  $\lambda = 40$ , and  $q = \pi$ . It is clear from the plot that good agreement between the numerical and analytical solution is observed.

earlier)

$$\frac{E_s}{\Omega} = -\frac{I_p}{\gamma}, \quad \text{where} \quad \gamma = \frac{ze\mu}{fH^2}. \quad (52)$$

In an effort to validate the analytical results, the same quantity, as given in Eq. (52) (i.e.,  $-I_p/\gamma$ ) has been calculated from the analytical perturbation method, although in the analytical solutions the inertia terms have been identically equated to zero.

Figure 2 depicts the comparative results for the variation of the quantity  $E_s/\Omega$ , upscaled by  $10^4$  with  $\delta$ . The values of the other relevant parameters are mentioned in the caption. We observe good agreement between the numerical and the analytical results. As expected, better agreement is observed when value of the parameter  $\delta$  (the perturbation parameter) is small. However, for the range of  $\delta$  as considered in the present figure, the relative percentage error always stays well below 0.5% (close to 0.2%), which falls within the acceptable limit of error. Following the present figure, it can thus be inferred that the present perturbation method offers accurate results within a small limiting error for the induced streaming potential.

### B. Implications of modulated wettability: Variations in induced streaming potential

We start our discussion with variations in the streaming potential with the surface modulations under consideration. In order to assess the relative importance of the slip modulation on the surfaces, we attempt to plot the ratio of the streaming potential with and without slip modulation on the surfaces. For determining the pertinent quantities we assume the slip

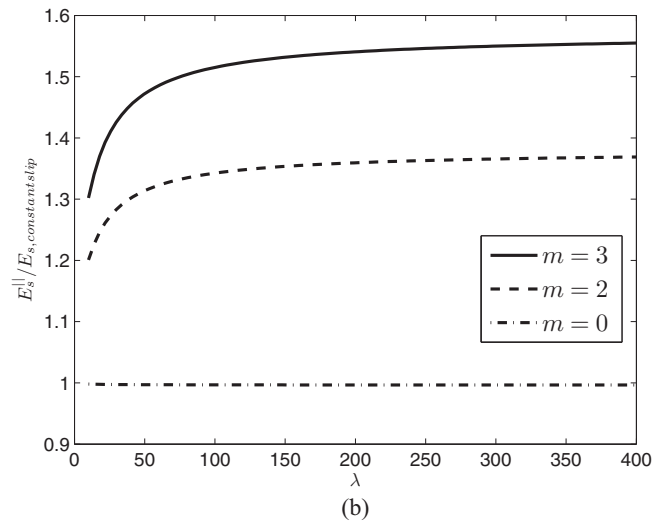
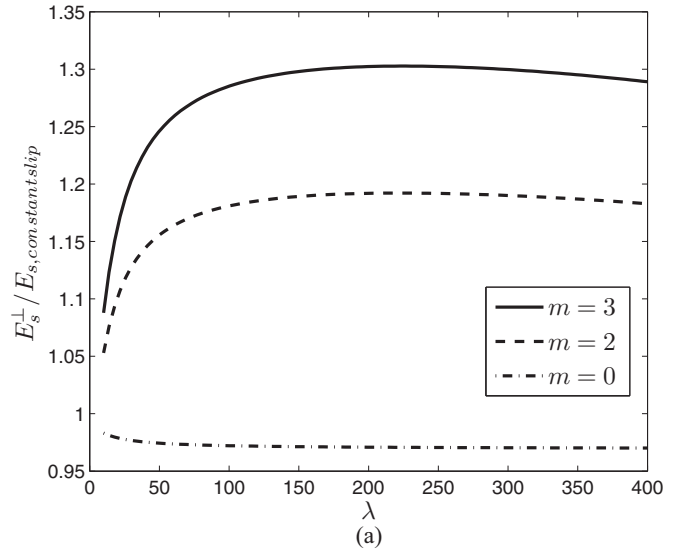


FIG. 3. (a)  $E_0^\perp$  vs  $\lambda$  for different values of  $m = 0, 2, 3$ . The other parameters are given by  $\theta = 0^\circ$ ,  $n = 1$ ,  $q = 1$ ,  $\delta = 0.4$ . (b)  $E_0^\parallel$  vs  $\lambda$  for different values of  $m = 0, 2, 3$ . The other parameters are the same as in (a).

length to be  $l_s = 0.1$  (the value of  $l_s$  has been assumed to be 0.1 throughout the analysis), which is same as the average slip for the cases with slip modulations on the surfaces. Additionally, the channel height has been assumed to be constant at  $H = 10^{-6}$  m, from here onwards.

Figures 3(a) and 3(b) demonstrate the variations in the streaming potential ratios in perpendicular ( $x$ ) and parallel ( $z$ ) directions with  $\lambda$ , respectively, for different values of  $m = 0, 2, 3$ . The values taken for the other parameters are mentioned in the caption. These figures indicate that the relative augmentation in the induced field in the  $x$  direction attains a maximum value for a certain value of  $\lambda$  and then diminishes again, whereas that for the  $z$  direction increases monotonically, although the rate of increment is arrested for high values of  $\lambda$ . The figures show that there is a decline in the induced streaming electric field, when the axially periodic part of the surface potential is made zero, i.e., when  $m = 0$ . Higher values of  $m$  significantly augment the induced fields,

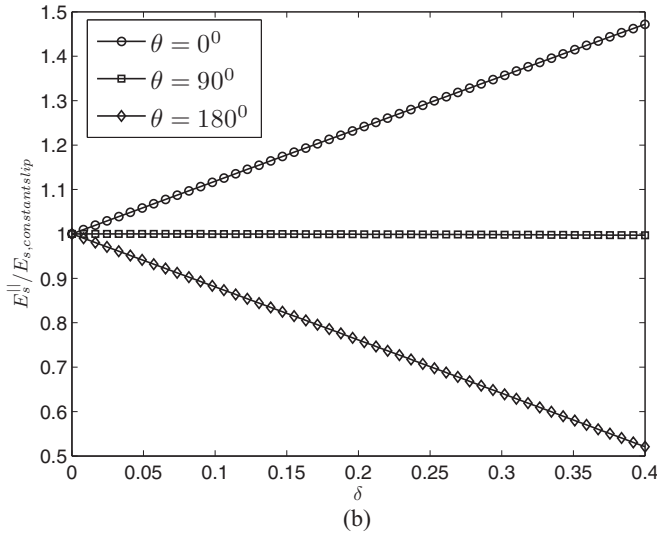
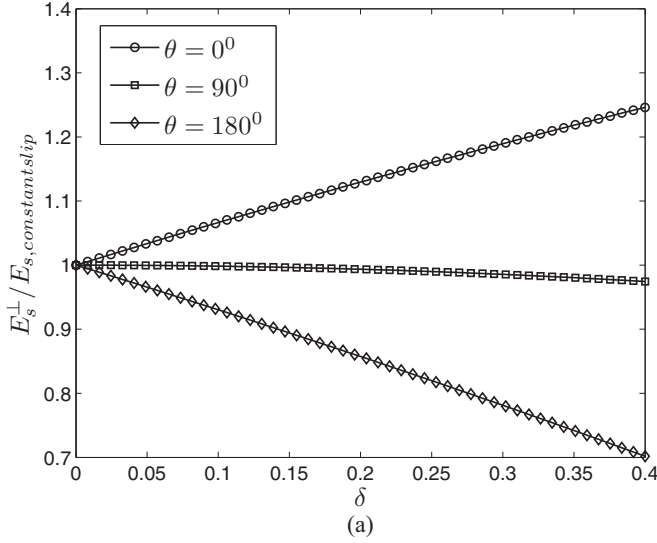


FIG. 4. (a)  $E_0^\perp$  vs  $\delta$  for different values of  $\theta = 0^\circ, 90^\circ$ , and  $180^\circ$ , while the other relevant parameters are given by  $\lambda = 50, m = 3, n = 1, q = 1$ . (b)  $E_0^\parallel$  vs  $\delta$  for different values of  $\theta = 0^\circ, 90^\circ$ , and  $180^\circ$ , with other parameters same as in (a).

which underlines the effects of modulated slip on the surfaces as apparent from Eqs. (14c) and (36b). The maximum relative augmentation in the  $x$ -direction field is obtained at values of  $\lambda$  close to 200, which signifies a Debye layer thickness of around 5 nm in a  $1\text{-}\mu\text{m}$  channel.

Figures 4(a) and 4(b) show the variation in the streaming potential ratios in the  $x$  and  $z$  directions, respectively, with  $\delta$  for different values of  $\theta = 0, 90^\circ$ , and  $180^\circ$ ; the values of the other relevant parameters are mentioned in the caption. The present figures prominently showcase the effects of modulated slip on the streaming potential. Quite intuitively, it follows from the expressions (14a)–(14d) and (36a)–(36c) that the streaming potential should increase with the amplitude of patterning for values of  $m$  greater than zero. Although the modulated slip also augments the streaming current due to the electric field, its value is much smaller as compared to the conduction current and the streaming current due to pressure.

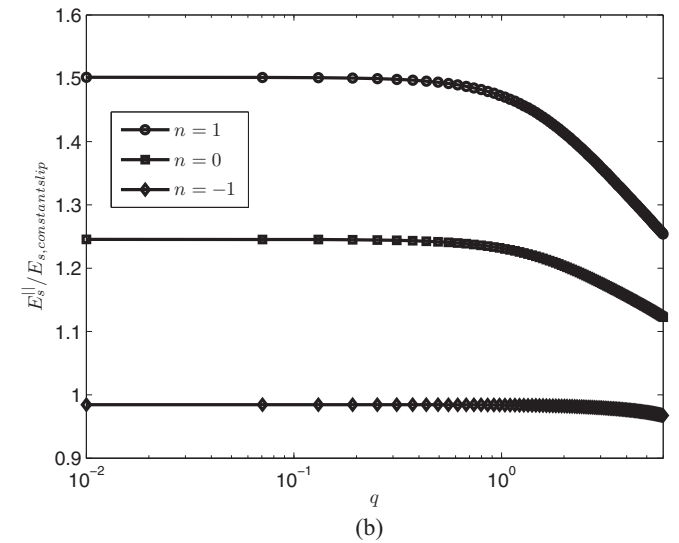
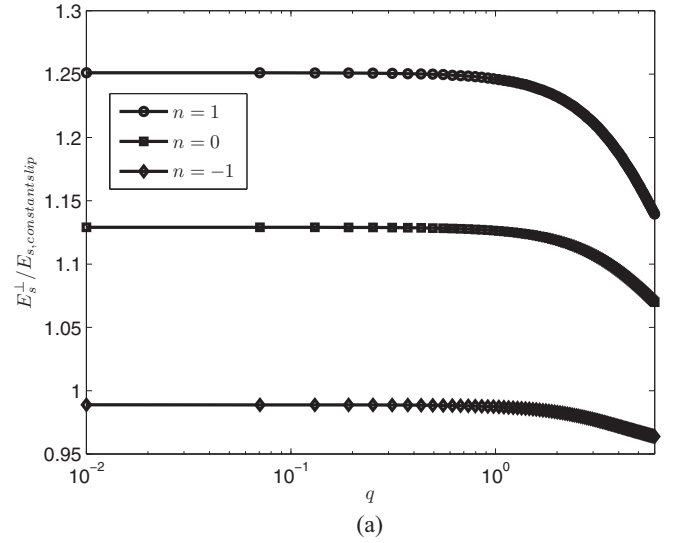


FIG. 5. (a)  $E_0^\perp$  vs  $q$  for different values of  $n = -1, 0, 1$ , with the other parameters being  $\lambda = 200, \theta = 0^\circ, m = 3, \delta = 0.4$ . (b)  $E_0^\parallel$  vs  $q$  for different values of  $n = -1, 0, 1$ . The other parameters are the same as in (a).

Hence, the variation of the pressure driven streaming current is predominantly reflected in the behavior of the induced field. It is interesting to note that, for a value of phase shift angle  $\theta > 90^\circ$ , the streaming potential drops significantly and the ratio becomes smaller than 1. This becomes apparent on reviewing Eqs. (14c) and (36b), where the sign of the  $O(\delta)$  term changes, thus making the streaming potential decrease with  $\delta$ .

Figures 5(a) and 5(b) depict the variation in the streaming potential ratios in  $x$  and  $z$  directions, respectively, with  $q$  for different values of  $n = -1, 0, 1$ ; the other relevant variables are mentioned in the caption. Note that a negative value of  $n$  indicates that the wettability modulation on the upper surface is out of phase with that of the lower surface. The values of the streaming electric field decrease with increasing patterning frequency, whereas higher values of  $n$  augment the induced field. It should be noted that, for low patterning frequencies the values remain almost constant. This indicates

the regime of lubrication approximation [35,52], where the characteristic length scale of variation in the axial direction is much larger as compared to the variation length scale across the channel. In cases of lubrication approximation, the flow characteristics have been shown by previous researchers [35,52] to be independent of the length scale of axial variation. As previously shown by Ajdari [35,52], under such assumptions, the equations of motion in  $i$ th direction can be written in the following form (nondimensional):

$$-\frac{\partial p}{\partial x_i} + \frac{\partial^2 u_{i,p}}{\partial y^2} = 0 \quad \text{and} \quad \frac{\partial^2 u_{i,e}}{\partial y^2} + \lambda^2 \psi = 0. \quad (53)$$

Here subscripts  $p$  and  $e$  denote contributions from the pressure driven and electro-osmotic flow, respectively, and  $x_1 \equiv x; x_2 \equiv z$ . The boundary conditions are given by Eq. (3a). The solutions to Eq. (53) can be expressed as (with  $n = 1$ )

$$u_{i,p} = \frac{1}{2} \left( -\frac{\partial p}{\partial x_i} \right) [y(1-y) + l_s \{1 + \delta \cos(qx + \theta)\}], \quad (54a)$$

$$u_{i,e} = 1 - \psi + \lambda \tanh(\lambda/2) l_s \{1 + \delta \cos(qx + \theta)\}. \quad (54b)$$

Note that the potential can be approximately expressed as

$$\psi \approx \frac{\cosh[\lambda(1/2 - y)]}{\cosh(\lambda/2)} (1 + m \cos qx). \quad (55)$$

Note that for the flow in the  $z$  direction  $-\frac{\partial p}{\partial x_i} = 1$ , although for flow in  $x$  direction, the same is periodic in nature, with  $\langle -\frac{\partial p}{\partial x} \rangle = 1$ , where,  $\langle \rangle$  denotes an average over the  $x$  direction. The streaming current can be calculated following the same method as in Eqs. (14a)–(14d) and the net effect can be extracted by taking average along the  $x$  direction.

For further clarity, we attempt to express our results in terms of experimentally realizable values. Toward this, we consider a typical microchannel setup with a height  $H \sim 1 \mu\text{m}$  and  $\zeta$  potential  $\zeta \sim 25 \text{ mV}$  (hence, we have considered  $m = 1$ ). We further note that typically reported slip length values lie in the order of tens to hundreds of nanometers [45,63,64], although much higher values of slip lengths have also been reported elsewhere [46,65–68]. Therefore, we consider a value of slip length  $l_s \sim 100 \text{ nm}$  and  $\delta = 0.4$  (with  $n = 1$ , i.e., equal slip patterning on both the walls). Additionally, we take the Debye layer thickness to be in the order of  $\sim 100 \text{ nm}$  and patterning frequency  $qH \sim 1$ –5. Previously, Van der Heyden *et al.* [20] executed experiments on generation of streaming potential with applied external pressure gradients in the order of  $\sim 1 \text{ bar/mm}$ , i.e.,  $10^8 \text{ Pa/m}$ . However, in the present study, we consider applied pressure gradients to be much smaller, on the order of  $10^5$ – $10^6 \text{ Pa/m}$  and the resulting streaming potential values lie in the range of  $\sim 10$ – $300 \text{ V/m}$ , the values of  $E^{\parallel}$  being slightly higher than those of  $E^{\perp}$ . Nevertheless, for higher pressure gradients, such as  $10^7 \text{ Pa/m}$  (although strictly speaking, the analysis is not quantitatively accurate for such high pressure gradients for flows in perpendicular direction), keeping other parameters constant, we obtain streaming potential in the tune of 2–3 kV/m.

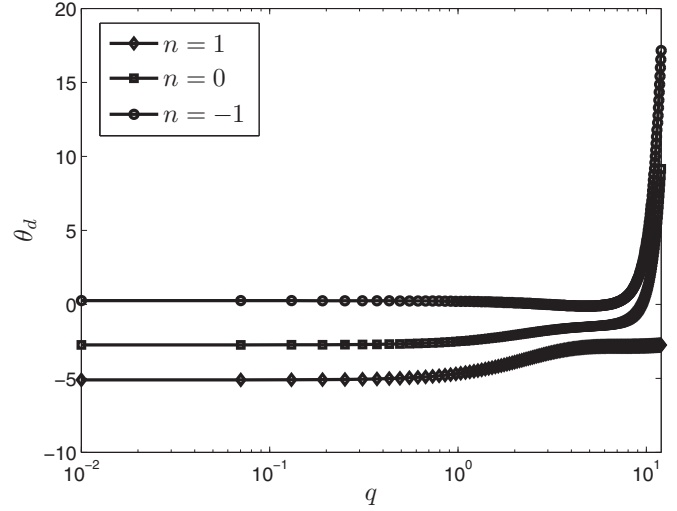


FIG. 6.  $\theta_d$  (in degrees) vs  $q$ , for different values of  $n = -1, 0, 1$ , with other parameters taken as  $\theta = 0^\circ$ ,  $m = 3$ ,  $\delta = 0.4$ ,  $\lambda = 200$ .  $\theta_d$  is the deviation angle, i.e., the angle between the applied pressure gradient and the induced streaming potential.

### C. Implications of anisotropy: Variations in the deviation angle

After a thorough discussion on the variation and relative augmentation of streaming potential, we now aim to study the implications of anisotropy induced by the surface modulations considered in the present study. Since the extent of anisotropy in the flow can be quantified through the deviation angle, we attempt to plot the same with the parameters dictating the modulation characteristics. As mentioned in the previous section, the effects of  $\delta$  and  $m$  on the deviation angle are somewhat intuitive as higher values of these parameters would lead to increased deviation angle. However, it might be interesting to investigate the effects of other relevant variables on the deviation angle to extract the extent of anisotropy. Note that we have taken the value of  $\theta_1$  to be  $\pi/4$  throughout the present section.

We start with variation in  $\theta_d$  with patterning frequency  $q$  for different values of  $n = -1, 0, 1$  (the other parameters are mentioned in the caption) in Fig. 6. This figure clearly shows the regime of lubrication approximation as the deviation angle remains virtually constant until  $q \sim 1$ . For higher values of  $q$ , anisotropy gets augmented drastically as the deviation angle reaches a value of almost  $18^\circ$  for  $n = -1$ . Interestingly, for  $n > 0$ , the deviation angle is negative, where the same is positive for  $n < 0$ , indicating the fact that for  $n > 0$ , the field in the parallel direction ( $E_0^{\parallel}$ ) is higher than the field in the perpendicular direction ( $E_0^{\perp}$ ) for the same applied pressure gradient, whereas for  $n < 0$  the reverse is true. Again, this can be attributed to the fact that the  $O(\delta)$  terms in expressions (14c) and (36b) change their sign when  $n$  changes its sign, which ultimately results in a drastic change in the induced streaming potential.

Figure 7 depicts the variation in  $\theta_d$  with  $\lambda$  for different values of  $m = 0, 1, 3$ , while the other relevant parameters have been mentioned in the caption. It can be observed that, for the presence of the axially varying component of surface potential the magnitude of deviation angle steadily increases, whereas the deviation angle, without the surface potential modulation,

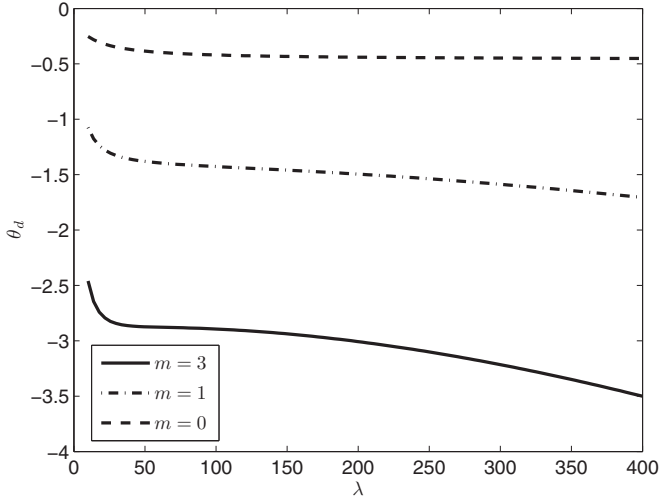


FIG. 7.  $\theta_d$ (in degrees) vs  $\lambda$ , for different values of  $m = 0, 1, 3$ . The other parameters have been taken as  $\theta = 0, n = 1, \delta = 0.4, q = 4$ .

is small ( $\sim 1^\circ$ ) and asymptotically tends towards a constant value for the range of  $\lambda$  taken for the present figure. Note that for  $m = 0$ , the  $O(\delta)$  term in Eqs. (14c) and (36b) disappears, which results in a reduced anisotropy. For the present figure, the induced field in the parallel direction remains slightly higher than that in the perpendicular direction.

Figure 8 demonstrates the variation in the deviation angle with  $\theta$ , the phase shift angle for different values of  $\lambda = 10, 50, 100, 300$  (other parameters have been mentioned in the caption). The most interesting feature in the present diagram is that, for every  $\lambda$  there exists a certain  $\theta$ , i.e., a certain phase shift angle, which results in zero deviation angle; i.e., the induced streaming potential is exactly oriented along the direction of the applied pressure gradient, albeit only for  $\theta_1 = \pi/4$ . We call this phase shift angle  $\theta_0$  and observe that, for  $\theta < \theta_0$ , the

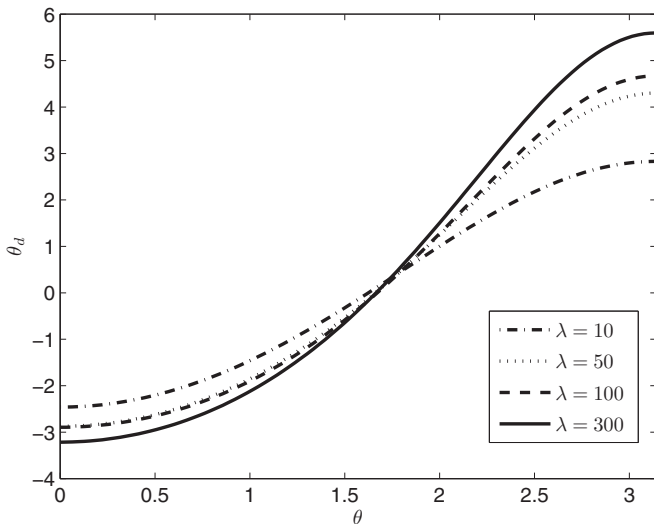


FIG. 8.  $\theta_d$ (in degrees) vs  $\theta$  (in radian), for different values of  $\lambda = 10, 50, 100, 300$ . The other parameters are given by  $m = 3, n = 1, \delta = 0.4, q = 4$ .

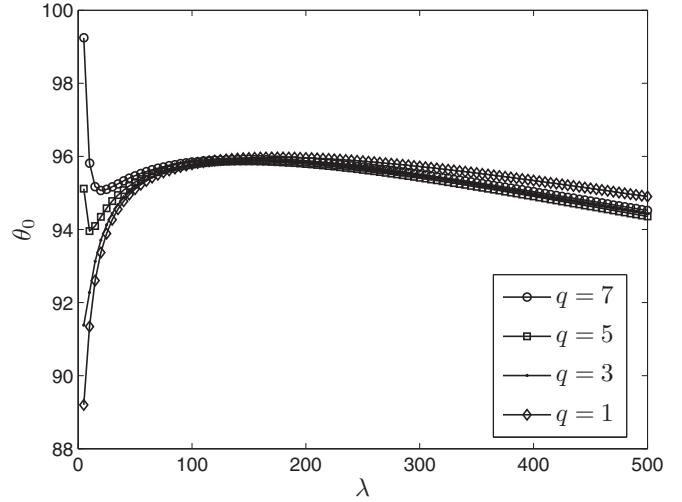


FIG. 9.  $\theta_0$ (in degrees) vs  $\lambda$ , for different values of  $q = 1, 3, 5, 7$ . The other parameters are given by  $m = 3, n = 1, \delta = 0.4$ . Note that  $\theta_0$  is the value of the phase shift angle  $\theta$  for which the streaming potential is oriented along the applied pressure gradient, for a value of  $\theta_1 = \pi/4$ .

field in the parallel direction remains stronger, whereas for  $\theta > \theta_0$ , that in the perpendicular direction becomes stronger.

In Fig. 9 we plot  $\theta_0$  with  $\lambda$  for different values of  $q = 1, 3, 5, 7$ . Interestingly,  $\theta_0$  shows two distinct kinds of behaviors here: First, for low values of patterning frequency,  $\theta_0$  increases with  $\lambda$ , reaches a maximum, and then drops slowly and monotonically; second, for high values of patterning frequency,  $\theta_0$  drops with increasing  $\lambda$ , then increases again before decreasing slowly for higher values of  $\lambda$ . It can be observed from the present figure that the values of  $\theta_0$  stay close to  $90^\circ$ , for a choice of  $\theta_1 = \pi/4$ . This figure reveals the fact that the streaming potential can be oriented along the applied pressure gradient by manipulating the concentration of the electrolyte in the solution and the phase shift angle between the wettability modulation and the surface potential modulation. One can also conclude from the present figure that by simply varying geometric parameters, like the channel height, the deviation angle can be removed. Thus, in essence, the presence of axial modulation of wettability and surface potential offers us great controllability over the directions and values of induced streaming potential.

#### IV. CONCLUSIONS

In the present study, we have evaluated the streaming potential induced by virtue of modulated slip and potential at the substrates of a fluidic confinement along the two orthogonal directions of the channel. We have also given an expression for the induced potential for an applied pressure gradient along any general direction. We have shown that in selective cases, the induced streaming electric field in both the directions are augmented with this combined modulation acting in tandem, whereas in other cases values for the same are decreased. By a careful review of the present analysis, the following conclusions can be drawn.

(i) The streaming electric field is augmented in the presence of axially modulated slip as compared to constant slip,

when only an axially varying component of the potential is applied at the walls.

(ii) Best attenuation in the induced field is obtained when the slip modulation and the modulations in the surface potential are in phase, whereas there is a relative drop in the same when the phase difference becomes  $\pi$ . However, this holds only for values of  $m, n > 0$ .

(iii) For selective cases, with  $n > 0$  (i.e., when the wettability modulations on the two surfaces are in phase) and  $\theta$  close to  $0^\circ$ , the induced potential along the parallel direction is stronger than that in the perpendicular direction, whereas the situation reverses when  $n < 0$ . One can thus control the direction of the streaming potential by finely tuning these parameters.

(iv) Higher patterning frequencies generally produce significantly higher values of deviation angle, which might reach as high as  $20^\circ$  or more for suitable choice of parameters.

(v) Taking  $n > 0$ , for each  $\lambda$ , i.e., for a given channel height to Debye length ratio, there exists a certain value of the phase shift angle  $\theta_0$ , for which the streaming potential is oriented along the applied pressure gradient, even if the

pressure gradient does not work along one of the orthogonal directions.

Implications of the results summarized as above may be far ranging. It has been well established in the literature that energy conversion efficiencies in microfluidic channels (having relatively thinner EDLs as compared to channel height) are comparatively poorer as compared to those realized for nanofluidic channels. The situation may get substantially worse when channels with modulated surface charges are employed, perhaps with the charge modulation obtained as an undesirable fabrication artifact. However, the present study indicates a possibility of augmenting the energy conversion efficiencies of such narrow fluidic channels to a considerable extent through a corresponding increase in the streaming potential, by remaining in the nonoverlapped EDL regime itself, with an exploitation of the combined interactions of modulations in surface potential and interfacial slip. In addition to this, anisotropic modulations also allow one to control the direction of the streaming potential by tuning various flow parameters finely, thus bearing huge scientific and technical implications.

- 
- [1] S. Chakraborty and S. Das, *Phys. Rev. E* **77**, 037303 (2008).
- [2] R. J. Hunter, *Zeta Potential in Colloid Science: Principles and Applications* (Academic Press, London, New York, 1981).
- [3] S. Das and S. Chakraborty, *Langmuir* **26**, 11589 (2010).
- [4] A. Bandopadhyay and S. Chakraborty, *Langmuir* **27**, 12243 (2011).
- [5] A. Bandopadhyay and S. Chakraborty, *Phys. Rev. E* **85**, 056302 (2012).
- [6] A. Bandopadhyay and S. Chakraborty, *Appl. Phys. Lett.* **101**, 043905 (2012).
- [7] R. Chein and J. Liao, *Electrophoresis* **28**, 635 (2007).
- [8] C. Davidson and X. Xuan, *J. Power Sources* **179**, 297 (2008).
- [9] J. Y. Mina, E. F. Hasselbrink, and S. J. Kim, *Sens. Actuators B* **98**, 368 (2004).
- [10] Y. Ren and D. Stein, *Nanotechnology* **19**, 195707 (2008).
- [11] C. Davidson and X. Xuan, *Electrophoresis* **29**, 1125 (2008).
- [12] D. Erickson and D. Li, *J. Colloid Interface Sci.* **237**, 283 (2001).
- [13] M.-S. Chun, T. S. Lee, and N.-W. Choi, *J. Micromech. Microeng.* **15**, 710 (2005).
- [14] S. K. Griffiths and R. H. Nilson, *Electrophoresis* **26**, 351 (2005).
- [15] E. Luaga, *Langmuir* **20**, 8924 (2004).
- [16] J. Chakraborty, S. Ray, and S. Chakraborty, *Electrophoresis* **33**, 419 (2012).
- [17] J. Chakraborty and S. Chakraborty, *Phys. Fluids* **23**, 082004 (2011).
- [18] J. Chakraborty and S. Chakraborty, *Phys. Fluids* **22**, 122002 (2010).
- [19] F. H. J. Van der Heyden, D. J. Bonthuis, D. Stein, C. Meyer, and C. Dekker, *Nano Lett.* **6**, 2232 (2006).
- [20] F. H. J. Van der Heyden, D. J. Bonthuis, D. Stein, C. Meyer, and C. Dekker, *Nano Lett.* **7**, 1022 (2007).
- [21] A. Paterson, M. Fermigier, P. Jenffer, and L. Limat, *Phys. Rev. E* **51**, 1291 (1995).
- [22] L. Dong, T. Nypel, M. Sterberg, J. Laine, and M. Alava, *Langmuir* **26**, 14563 (2010).
- [23] S. Bhattacharya, A. Datta, J. M. Berg, and S. Gangopadhyay, *J. Microelectromech. Syst.* **14**, 590 (2005).
- [24] J. A. Lim, J. H. Cho, Y. Jang, J. T. Han, and K. Cho, *Thin Solid Films* **515**, 2079 (2006).
- [25] M. Kogoma, H. Kasai, K. Takahashi, T. Moriwaki, and S. Okazaki, *J. Phys. D* **20**, 147 (1987).
- [26] F. V. Monteleone, C. Canale, G. Caputo, P. D. Cozzoli, R. Cingolani, D. Fragouli, and A. Athanassiou, *Langmuir* **27**, 8522 (2011).
- [27] J. C. Love, L. A. Estroff, J. K. Kriebel, R. G. Nuzzo, and G. M. Whitesides, *Chem. Rev.* **105**, 1103 (2005).
- [28] X. Wu and G. Shi, *Nanotechnology* **16**, 2056 (2005).
- [29] F. Zhou and W. T. S. Huck, *Chem. Commun.* 5999 (2005).
- [30] M. Jin, M. X. Feng, L. Feng, T. Sun, J. Zhai, T. Li, and L. Jiang, *Adv. Mater.* **17**, 1977 (2005).
- [31] T. Sun, G. Wang, L. Feng, B. Liu, Y. Ma, L. Jiang, and D. Zhu, *Angew. Chem., Int. Ed.* **43**, 357 (2004).
- [32] Z. Guo, F. Zhou, J. Hao, and W. Liu, *J. Am. Chem. Soc.* **127**, 15670 (2005).
- [33] Z. Zheng, O. Azzaroni, F. Zhou, and W. T. S. Huck, *J. Am. Chem. Soc.* **128**, 7730 (2006).
- [34] U. Ghosh and S. Chakraborty, *Phys. Rev. E* **85**, 046304 (2012).
- [35] E. Brunet and A. Ajdari, *Phys. Rev. E* **73**, 056306 (2006).
- [36] A. Ajdari, *Phys. Rev. E* **53**, 4996 (1996).
- [37] A. Ajdari, *Phys. Rev. Lett.* **75**, 755 (1995).
- [38] A. D. Stroock, M. Weck, D. T. Chiu, W. T. S. Huck, P. J. A. Kenis, R. F. Ismagilov, and G. M. Whitesides, *Phys. Rev. Lett.* **84**, 3314 (2000).
- [39] D. Erickson and D. Li, *Langmuir* **18**, 1883 (2002).
- [40] S. Ghosal, *J. Fluid Mech.* **459**, 103 (2002).
- [41] J.-B. Zhang, G.-W. He, and F. Liu, *Phys. Rev. E* **73**, 056305 (2006).
- [42] C.-K. Chen and C.-C. Cho, *Chem. Eng. Sci.* **63**, 3081 (2008).
- [43] C.-C. Chang and R.-J. Yang, *Phys. Rev. E* **77**, 056311 (2008).

- [44] F. Tian, B. Li, and D. Y. Kwok, *Langmuir* **21**, 1126 (2005).
- [45] D. Naga Neehar and S. Chakraborty, *Microfluid Nanofluid* **12**, 395 (2012).
- [46] S. C. Hendy, M. Jasperse, and J. Burnell, *Phys. Rev. E* **72**, 016303 (2005).
- [47] C.-O. Ng and C. Y. Wang, *Microfluid. Nanofluid.* **8**, 361 (2010).
- [48] C.-O. Ng and C. Y. Wang, *J. Fluids Eng.* **133**, 014502 (2011).
- [49] S. S. Bahga, M. Z. Bazant, and O. I. Vinogradova, *J. Fluid Mech.* **644**, 245 (2010).
- [50] C.-O. Ng and H. C. W. Chu, *Phys. Fluids* **23**, 102002 (2011).
- [51] C.-O. Ng and C. Y. Wang, *Phys. Fluids* **21**, 013602 (2009).
- [52] A. Ajdari, *Phys. Rev. E* **65**, 016301 (2001).
- [53] S. Schmieschek, A. V. Belyaev, J. Harting, and O. I. Vinogradova, *Phys. Rev. E* **85**, 016324 (2012).
- [54] F. Feuillebois, M. Z. Bazant, and O. I. Vinogradova, *Phys. Rev. E* **82**, 055301(R) (2010).
- [55] A. V. Belyaev and O. I. Vinogradova, *Phys. Rev. Lett.* **107**, 098301 (2011).
- [56] E. S. Asmolov, S. Schmieschek, J. Harting, and O. I. Vinogradova, *Phys. Rev. E* **87**, 023005 (2013).
- [57] P. Six and K. Kamrin, *Phys. Fluids* **25**, 021703 (2013).
- [58] M. Sbragaglia and A. Prosperetti, *Phys. Fluids* **19**, 043603 (2007).
- [59] H. Zhao, *Phys. Fluids* **23**, 022003 (2011).
- [60] N. A. Mortensen, L. H. Olesen, L. Belmon, and H. Bruus, *Phys. Rev. E* **71**, 056306 (2005).
- [61] M. Z. Bazant, K. Thornton, and A. Ajdari, *Phys. Rev. E* **70**, 021506 (2004).
- [62] A. D. Stroock, S. K. Dertinger, G. M. Whitesides, and A. Ajdari, *Anal. Chem.* **74**, 5306 (2002).
- [63] Y. Zhu and S. Granick, *Phys. Rev. Lett.* **88**, 106102 (2002).
- [64] E. Bonaccorso, H. J. Butt, and V. S. J. Craig, *Phys. Rev. Lett.* **90**, 144501 (2003).
- [65] C. Lee, C.-H. Choi, and C.-J. Kim, *Phys. Rev. Lett.* **101**, 064501 (2008).
- [66] C.-H. Choi, U. Ulmanella, J. Kim, C.-M. Ho, and C.-J. Kim, *Phys. Fluids* **18**, 087105 (2006).
- [67] P. Tsai, A. M. Peters, C. Pirat, M. Wessling, R. G. H. Lammertink, and D. Lohse, *Phys. Fluids* **21**, 112002 (2009).
- [68] J. Baudry, E. Charlaix, A. Tonck, and D. Mazuyer, *Langmuir* **17**, 5232 (2001).